Local signaling specifies tissue-resident fibroblasts from multipotent sclerotome progenitors in zebrafish

Roger C. Ma[1], Katrinka M. Kocha[1], and Peng Huang[1]*

[1] Department of Biochemistry and Molecular Biology, Cumming School of Medicine, Alberta Children's Hospital Research Institute, University of Calgary, 3330 Hospital Drive, Calgary, Alberta, Canada T2N 4N1

* Correspondence should be addressed to PH.

Email: huangp@ucalgary.ca
Tel: 403-220-4612

Running title: Diversification of tissue-resident fibroblasts

Keywords: Fibroblasts, Sclerotome, Collagen, BMP signaling, Fin mesenchymal cells, Zebrafish

ABSTRACT

Fibroblasts play an important role in maintaining tissue integrity by secreting components of the extracellular matrix and initiating response to injury. Although the function of fibroblasts has been extensively studied in adults, the embryonic origin and diversification of different fibroblast subtypes during development remain largely unexplored. Using zebrafish as a model, we show that the sclerotome, a sub-compartment of the somite, is the embryonic source of multiple fibroblast populations, including tenocytes (tendon fibroblasts), blood vessel associated fibroblasts, and fin mesenchymal cells. High resolution imaging shows that different fibroblast subtypes occupy unique anatomical locations with distinct morphologies. Photoconversion-based cell lineage analysis reveals that sclerotome progenitors at different dorsal-ventral and anterior-posterior positions display distinct differentiation potentials. Single cell clonal analysis suggests that sclerotome progenitors are multipotent, and the fate of their daughter cells is biased by their migration paths and relative positions. Using a small molecule inhibitor, we show that BMP signaling is required for the development of fin mesenchymal cells in the peripheral fin fold. Together, our work demonstrates that the sclerotome contains multipotent progenitors that respond to local signals to generate a diverse population of tissue-resident fibroblasts.

AUTHOR SUMMARY

Fibroblasts are present in most organs in our body. They not only provide structural support to corresponding tissues, but also play important roles in wound healing and tissue fibrosis. Although the function of fibroblasts has been well appreciated, how different tissue-resident fibroblasts emerge during embryonic development is still poorly understood. Using the zebrafish model, we identify the sclerotome, a sub-compartment of the embryonic somite, as the main source of multiple fibroblast populations. Different fibroblast subtypes display distinct morphologies and locate at unique positions to support different tissues, including the muscles, blood vessels and the fin fold. Using cell tracing in live animals, we find that single sclerotome progenitors are able to generate more than one type of fibroblasts. The differentiation potential of sclerotome progenitors is biased by their initial locations in the trunk as well as their migration directions and relative positions. Local BMP signaling in the fin fold is essential for the proper development of sclerotome derived fin mesenchymal cells. Together, our results show that local microenvironment contributes to the diversification of multipotent sclerotome progenitors into distinct fibroblast subtypes.

54 **INTRODUCTION**

55

56 Fibroblasts are connective tissue cells that are present in most organs in animals. They are
57 traditionally viewed as tissue support cells by synthesizing and remodeling extracellular matrix (ECM)
58 components. Recent work has shown that tissue-resident fibroblasts also play important regulatory
59 roles in wound healing, inflammation, tumor microenvironment, and tissue fibrosis (Kalluri, 2016;
60 Kendall and Feghali-Bostwick, 2014; Thulabandu et al., 2018). Although fibroblasts are historically
61 viewed as a homogenous population of cells, recent work using single-cell RNA sequencing (scRNA-
62 seq) has revealed a high level of heterogeneity in the fibroblast population from different tissues as
63 well as within the same tissue (Muhl et al., 2020; Tabib et al., 2018; Xie et al., 2018). It thus raises the
64 question how different fibroblast subtypes are generated during embryonic development.
65 One mechanism to diversify fibroblast populations is through contributions from multiple
66 embryonic sources. Previous studies suggest that fibroblasts of the same tissue can have
67 heterogeneous embryonic origins. For example, in avian and mouse embryos, dermal fibroblasts in
68 the head are of neural crest origin, while dermal fibroblasts in the dorsal and ventral trunk originate
69 from the somite and the lateral plate mesoderm, respectively (Thulabandu et al., 2018). Similarly,
70 during heart development in chick and mouse embryos, most cardiac fibroblasts originate from lateral
71 plate mesoderm derived epicardium, while a small population arises from an endothelial/endocardial
72 lineage (Tallquist, 2020).
73 The somite is the embryonic source of many tissue support cells, including fibroblasts. During
74 development, the somite forms three separate domains: the dermatome, the myotome, and the
75 sclerotome. The sclerotome contributes to the axial skeleton and cartilage of the animal. Work in
76 mouse and chick has shown that the sclerotome is the developmental origin of tendon fibroblasts
77 (tenocytes) (Brent et al., 2003; Schweitzer et al., 2001) and vascular smooth muscle cells (Pouget et
78 al., 2008; Wiegreffe et al., 2007). In zebrafish, the sclerotome has a unique bipartite organization and
79 contributes to tenocytes, perivascular fibroblasts, and pericytes in a stereotypical manner (Ma et al.,
80 2018; Rajan et al., 2020). It raises the question about the cellular mechanisms that govern the
81 diversification of fibroblast subtypes from sclerotome progenitors.
82 In fish and amphibians, fin mesenchymal cells are a population of fibroblasts present in the larval
83 fin fold. They express many ECM components to provide structural support to the developing fin fold
84 (Durán et al., 2011; Feitosa et al., 2012). However, the developmental origin of fin mesenchymal cells
85 has been controversial. Dye labeling experiments in *Xenopus* and zebrafish suggest that the neural
86 crest contributes to the fin mesenchyme (Smith and Hall, 1990; Smith et al., 1994). However, later
87 experiments in *Xenopus* suggest that the mesoderm also contributes to fin mesenchymal cells in both

88 the dorsal and ventral fin (Garriock and Krieg, 2007; Tucker and Slack, 2004). Similarly, cell
89 transplantation experiments in axolotls reveal dual origin of the fin mesenchyme from both the neural
90 crest and the somites (Sobkow et al., 2006). More recent work using genetic lineage tracing in fish
91 (zebrafish) and amphibians (*Xenopus* and axolotl) supports a model where fin mesenchymal cells
92 originate exclusively from the mesoderm with no contribution from the neural crest lineage (Lee et al.,
93 2013; Taniguchi et al., 2015). In particular, the dermomyotome compartment of the somite has been
94 suggested to be the source of fin mesenchymal cells in zebrafish (Lee et al., 2013).
95 Here, we show that the sclerotome is a major source of multiple distinct fibroblast populations in
96 zebrafish embryos. Different sclerotome derived fibroblast subtypes display unique morphologies and
97 occupy distinct anatomical locations. In vivo time-lapse imaging and single cell clonal analysis reveal
98 that sclerotome progenitors are multipotent, and their differentiation potential is determined by their
99 positions as well as their migratory patterns. Specifically, fin mesenchymal cells are specified by local
100 BMP signals at the peripheral fin fold. Together, our results suggest that distinct fibroblast subtypes
101 are specified from multipotent sclerotome progenitors by local cellular environments.

102 **RESULTS**

103

104 **The zebrafish sclerotome generates distinct fibroblast subtypes**

105 To explore the lineage potential of the sclerotome, we developed a sclerotome-specific reporter
106 line, *nkx3.1:Gal4; UAS:NTR-mCherry* (*nkx3.1*$^{NTR\text{-}mCherry}$, similar designations are used for all Gal4/UAS
107 transgenic lines in this paper) (Ma et al., 2018). Due to the perdurance of the mCherry protein, we
108 were able to label the initial sclerotome domains as well as all their descendants. We crossed
109 *nkx3.1*$^{NTR\text{-}mCherry}$ to the endothelial reporter *kdrl:EGFP* to examine the different populations of
110 sclerotome derived cells at 2 dpf (days post fertilization). Based on their anatomical locations, we
111 broadly defined four main groups of mCherry^{+} cells from the sclerotome lineage (Fig 1A and 1B): 1)
112 cells located in both dorsal and ventral fin folds; 2) cells closely associated with blood vessels in the
113 trunk, including the dorsal longitudinal anastomotic vessel (DLAV), intersegmental vessels (ISV), the
114 dorsal aorta (DA), and the caudal vein plexus (CVP); 3) tenocytes between neighboring somites as
115 we have previously described (Ma et al., 2018); and 4) interstitial cells located in the space between
116 the notochord, the spinal cord and muscles. It is worth noting that the *nkx3.1*$^{NTR\text{-}mCherry}$ line also drove
117 expression in some muscle cells (Ma et al., 2018) and in some cuboidal cells at the edge of the fin
118 fold (Fig 1B), neither of which were derived from the sclerotome lineage. We have previously shown
119 that both tenocytes and ISV-associated perivascular fibroblasts express the pan-fibroblast markers
120 such as *col1a2* and *col5a1* (Ma et al., 2018; Rajan et al., 2020). We asked whether other sclerotome
121 derived cells are also fibroblasts. Indeed, all four groups of *nkx3.1*$^{NTR\text{-}mCherry}$-expressing cells were
122 positive for *col1a2:GFP*, a pan-fibroblast reporter, at 2 dpf (Fig S1C). This result suggests that the
123 sclerotome is the embryonic source of multiple types of fibroblasts in zebrafish.

124 At 2 dpf, the fin fold is subdivided into two lobes (Parichy et al., 2009) (Fig S1A). The major lobe
125 arises from the dorsal edge of somite 7, wraps around the trunk and the tail, and ends at the ventral
126 edge at somite 18 where it meets the end of the yolk extension. The minor lobe extends ventrally
127 underneath the yolk extension. In *nkx3.1*$^{NTR\text{-}mCherry}$ embryos, mCherry^{+} cells can be seen populating
128 both the dorsal and ventral regions in the major lobe of the fin fold (Fig 1B and S1B). Using a mosaic
129 *col1a2:Gal4; UAS:Kaede* line (referred to as *col1a2*^{Kaede}) (Sharma et al., 2019), we visualized the cell
130 morphology at high resolution (Fig 1C). These Kaede^{+} fin cells were characterized by extensive "tree-
131 like" cellular processes projecting towards the periphery of the fin fold (Fig 1B and 1C). The location,
132 morphology, as well as the marker expression (shown later) suggest that these sclerotome derived fin
133 fold residing cells correspond to fin mesenchymal cells as previously described (Feitosa et al., 2012;
134 Lee et al., 2013). Interestingly, mCherry^{+} fin mesenchymal cells were absent in the fin fold at the tip of

135 the tail and the minor lobe (Fig S1B), suggesting that the sclerotome is not the only lineage that gives
136 rise to fin mesenchymal cells.
137 Within the zebrafish trunk, many sclerotome derived fibroblasts were found associated with
138 different vascular beds (Fig 1A and 1B). We have previously described ISV-associated perivascular
139 fibroblasts, characterized by a globular cell body with a few short processes extended around the ISV
140 (Rajan et al., 2020). By contrast, fibroblasts associated with DLAV or DA (referred to as DLAV
141 fibroblasts and DA fibroblasts, respectively) were more elongated along the long axis of the blood
142 vessel (Fig 1B and 1C). The CVP is a transient venous network with a stereotypical "honeycomb-like"
143 structure. Fibroblasts marked by *nkx3.1*$^{NTR\text{-}mCherry}$ were found occupying the space in the honeycomb
144 pockets of the CVP (Fig 1B). Mosaic labeling with *col1a2*^{Kaede} revealed that individual Kaede^{+} cells
145 had a small and elongated cell body with long cellular processes along the underlying endothelium
146 and sometimes across the honeycomb pocket (Fig 1C). Their location and morphology suggest that
147 these CVP-associated fibroblasts are previously described stromal reticular cells (SRCs) (Murayama
148 et al., 2015).
149 Finally, tenocytes and interstitial fibroblasts were two fibroblast subtypes that populated in the
150 trunk region but were not closely associated with blood vessels. We have previously shown that
151 tenocytes, marked by *scxa* and *tnmd* expression, are located along the myotendinous junction (MTJ),
152 extending long cellular processes into the intersomitic space (Fig 1B and 1C) (Ma et al., 2018). By
153 contrast, interstitial fibroblasts were scattered throughout the interstitial space, displaying varied
154 morphology (Fig 1B and 1C). Together, our results show that the sclerotome generates multiple types
155 of fibroblasts in the zebrafish trunk, supporting different tissues, such as muscles, blood vessels and
156 the fin fold. These fibroblast subtypes display unique morphologies locating in distinct anatomical
157 locations, some of which can be defined by specific marker expression.
158
159 **Both dorsal and ventral sclerotome domains give rise to multiple types of fibroblasts**
160 We have previously shown that the sclerotome is comprised of a dorsal and ventral domain, both
161 of which contribute to tenocytes and perivascular fibroblasts (Ma et al., 2018; Rajan et al., 2020). We
162 asked how each sclerotome domain contributes to different fibroblast subtypes. Taking advantage of
163 the photoconvertible Kaede protein, we generated the *nkx3.1:Gal4; UAS:Kaede* line (referred to as
164 *nkx3.1*^{Kaede}) to perform lineage tracing on sclerotome domains (Fig 2A). Either the dorsal or ventral
165 sclerotome domain of a single somite was photoconverted from Kaede^{green} to Kaede^{red} at 24 hpf
166 (hours post fertilization). We then determined the fate of Kaede^{red} cells after 24 hours based on their
167 anatomical locations and cell morphologies. For the ventral sclerotome, we also compared the lineage
168 between anterior somites before the end of yolk extension (somites 16-18) and posterior somites

169 (somites 23-25) as stromal reticular cells and ventral fin mesenchymal cells were only present in the
170 more posterior region of the fish.
171 First, we labeled the dorsal sclerotome domain by Kaede photoconversion at 24 hpf. The
172 presence of some small projections from these Kaede^{red} cells suggests that cell migration may be
173 initiating at this stage (Fig 2B). By 48 hpf, multiple Kaede^{red} cells can be seen populating the dorsal
174 region of the fish (Fig 2B). Based on their morphology and location relative to the vasculature, we
175 determined that the cell types generated by the dorsal sclerotome domain included dorsal fin
176 mesenchymal cells, DLAV fibroblasts, tenocytes, ISV-associated perivascular fibroblasts, and
177 interstitial fibroblasts. All dorsal sclerotome derived cells were restricted within the upper half of the
178 zebrafish trunk dorsal to the notochord.
179 We next carried out photoconversion experiments to mark the ventral sclerotome domain with
180 Kaede^{red} at 24 hpf. Similar to the dorsal domain, small cellular projections were visible from Kaede^{red}
181 cells, suggesting that both dorsal and ventral sclerotome progenitors initiate their migration at the
182 same stage (Fig 2C). Interestingly, in anteriorly converted somites (Fig 2C, top panels), cellular
183 projections pointed exclusively to the dorsal direction, while in posteriorly converted somites (Fig 2C,
184 bottom panels), cellular projections can be seen pointing both dorsally and ventrally. This result
185 suggests that the migration pattern is potentially different in ventral sclerotome progenitors between
186 anterior and posterior somites, which likely accounts for cells generated in the CVP and ventral fin fold
187 region. In anterior somites, the ventral sclerotome generated cells in the trunk, including tenocytes,
188 perivascular fibroblasts, and interstitial fibroblasts by 48 hpf (Fig 2C, top panels). Importantly, Kaede^{red}
189 descendants were only found dorsal to their starting position, and therefore, no SRCs or ventral fin
190 mesenchymal cells were labeled. In contrast, in posterior somites, the ventral sclerotome domain
191 gave rise to both cells in the trunk, including tenocytes, perivascular fibroblasts, and interstitial
192 fibroblasts, as well as cells in the periphery ventral to the photoconverted region, such as SRCs
193 associated with the CVP and fin mesenchymal cells in the ventral fin fold. All cells generated by the
194 ventral sclerotome domain were restricted within approximately the ventral 2/3 of the zebrafish trunk.
195 Together, our result suggests that both dorsal and ventral sclerotome domains are able to
196 generate multiple fibroblast subtypes, but the progenitors in each domain generate an anatomically
197 restricted population of cells according to their dorsal-ventral and anterior-posterior positions.
198
199 **Fate of dorsal sclerotome progenitors is determined by the migration direction**
200 Both dorsal and ventral sclerotome domains contribute to multiple types of fibroblasts. It is
201 possible that sclerotome progenitors are multipotent, or alternatively, individual progenitors are "fate-
202 restricted" to differentiate into a specific subtype of fibroblast. To distinguish these two possibilities, we

203 performed single cell clonal analysis on sclerotome progenitors as previously described (Sharma et
204 al., 2019). We focused on the smaller dorsal domain to ensure precise single cell photoconversion
205 and accurate cell tracing. We selected *nkx3.1*^{Kaede} fish with more mosaic Kaede expression to
206 minimize the photoconversion of multiple sclerotome progenitors. At 24 hpf, a single Kaede^{green} cell in
207 the dorsal domain between somites 16 and 18 was photoconverted to Kaede^{red} (Fig 3A). We then
208 imaged the same fish after 24 hours to determine the identity of Kaede^{red} descendants. Most clones
209 (35/42, 83%) contained at least 2 daughter cells, suggesting at least one cell division during the 24-
210 hour period (Fig 3B). From a total of 42 dorsal sclerotome progenitors, 38% of them (16/42) produced
211 clones with at least 2 fibroblast subtypes, and 2% (1/42) generated 3 different types of fibroblasts (Fig
212 3C). This result suggests that most dorsal sclerotome progenitors are at least bi-potent and possibly
213 multipotent at 24 hpf. Consistent with the domain tracing, we found that dorsal sclerotome progenitors
214 gave rise to all 4 types of fibroblasts, including dorsal fin mesenchymal cells, tenocytes, blood vessel
215 associated fibroblasts, and interstitial fibroblasts (Fig 3D). As described earlier, the individually labeled
216 Kaede^{red} cells at 24 hpf often had small projections that pointed either dorsally or ventrally, likely
217 corresponding to their migration direction. To correlate the progenitor morphology with their lineage
218 potential, we categorized different fibroblasts into two types based on their final positions (Fig 3A). In
219 the type I group, fibroblasts are located dorsal to the somite, and these include dorsal fin
220 mesenchymal cells and DLAV fibroblasts. Type II cells, such as tenocytes, ISV associated
221 perivascular fibroblasts, and interstitial fibroblasts, are located medial to the somite within the trunk
222 region. Interestingly, progenitors with initial dorsal projections predominantly generated type I cells
223 (13/14, 93%), whereas cells projecting ventrally more likely gave rise to type II cells (11/19, 58%) than
224 type I cells (3/19, 16%), and sometimes generated cells of both types (5/19, 26%) (Fig 3E and 3F). It
225 is important to note that ventral projecting progenitors at 24 hpf never generated dorsal fin
226 mesenchymal cells and all type I cells generated by this group were DLAV fibroblasts found along the
227 ventral side of the DLAV (Fig 3F). Together, our results suggest that individual dorsal sclerotome
228 progenitors at 24 hpf are still multipotent; however, their migration direction likely restricts the types of
229 cells they differentiate into.
230
231 **Fate of ventral sclerotome progenitors is determined by the position along the migratory path**
232 In posterior somites, some ventral sclerotome progenitors migrate ventrally towards the CVP
233 region to generate SRCs and ventral fin mesenchymal cells. To visualize this dynamic process, we
234 performed time-lapse imaging in *kdrl:EGFP; nkx3.1*$^{NTR\text{-}mCherry}$ embryos from 25 to 50 hpf (Fig 4 and
235 Video S1). At 25 hpf, some migrating mCherry^{+} progenitors can already be found ventral to the
236 somite. These cells migrated ventrally towards the fin fold as more mCherry^{+} cells emerged from the

237 ventral somite and joined the migration. To better describe the position of migrating cells, we referred
238 to cells at the very front edge of the migration as “leading cells”, while all cells behind were called
239 “lagging cells”. We observed a stereotypical migration pattern whereby mCherry^{+} cells “marched”
240 ventrally in an orderly fashion and individual cells did not pass other cells that were ahead. This
241 orderly migration was largely maintained even in the event of cell divisions. As a result, descendants
242 of leading cells remained at the front of the migration throughout the movie and formed ventral fin
243 mesenchymal cells, whereas descendants of lagging cells mostly generated SRCs associated with
244 the CVP. This result suggests that the fate of ventral sclerotome progenitors is determined by their
245 position along the migratory path.
246 To further compare the lineage potential between the leading and lagging cells, we performed
247 single cell clonal analysis using *nkx3.1*^{Kaede} fish (Fig 5A). Single ventrally migrating Kaede^{green}
248 progenitors between somites 21-25 were photoconverted to Kaede^{red} at 24 hpf, and their descendants
249 were imaged after 24 hours. Similar to our time-lapse movies, the majority of photoconverted leading
250 cells generated only ventral fin mesenchymal cells (17/20, 85%), but a small number of them gave
251 rise to both SRCs and ventral fin mesenchymal cells (3/20, 15%) (Fig 5B and 5C). Interestingly,
252 leading cells never generated SRCs only. By contrast, 41% of lagging cells generated only SRCs
253 (9/22), while 36% generated both ventral fin mesenchymal cells and SRCs (8/22), and 23% produced
254 only ventral fin mesenchymal cells (5/22) (Fig 5B and 5C). It should be noted that the closer a lagging
255 cell was to a leading cell, the more likely it generated a ventral fin mesenchymal cell, suggesting that
256 lagging cells have the potential to differentiate into fin mesenchymal cells in the appropriate
257 environment. Combining time-lapse imaging and single cell tracing, our results suggest that the
258 relative position along the migratory path biases the fate of these sclerotome derived cells.
259
260 **Fin mesenchymal cells respond to local BMP ligands**
261 Our results have shown that the sclerotome contributes to fin mesenchymal cells in both dorsal
262 and ventral fin folds. Previous studies have shown that fin mesenchymal cells are marked by
263 *hemicentin2* (*hmcn2*) and *fibulin1* (*fbln1*), while the neighboring cell layer of apical epidermal cells is
264 labelled by *hmcn2* and *fras1* (Carney et al., 2010; Feitosa et al., 2012; Lee et al., 2013) (Fig 6A).
265 Indeed, double staining revealed two juxtaposing cell layers in the fin fold: *hmcn2*$^{+}$*fbln1*$^{+}$ fin
266 mesenchymal cells in the proximal layer and *hmcn2*$^{+}$*fras1*$^{+}$ apical epidermal cells in the distal layer
267 (Fig 6B). As expected, double staining in *nkx3.1*$^{NTR\text{-}mCherry}$ embryos showed that mCherry^{+} cells in the
268 fin fold co-expressed *fbln1* but not *fras1* (Fig 6C), confirming that the sclerotome contributes to fin
269 mesenchymal cells, a specific cell population in the fin fold.

270 We hypothesized that the development of fin mesenchymal cells is mediated by local signals in
271 the fin fold. To test this model, we performed expression analysis to identify signaling ligands enriched
272 in the fin fold. Interestingly, we found that a number of *bmp* genes, including *bmp2b*, *bmp4*, and
273 *bmp6*, were expressed specifically in *fras1*$^{+}$ apical epidermal cells, adjacent to *fbln1*$^{+}$ fin mesenchymal
274 cells (Fig 6D and S2). Accordingly, *nkx3.1*$^{NTR\text{-}mCherry}$-positive fin mesenchymal cells were positioned
275 along a layer of *bmp4*-expressing cells (Fig 6C). This result suggests that BMP ligands secreted from
276 apical epidermal cells might activate BMP signaling in fin mesenchymal cells. To test this possibility,
277 we crossed the *nkx3.1*$^{NTR\text{-}mCherry}$ line to the *BRE:GFP* reporter to label BMP responsive cells (Collery
278 and Link, 2011). At 2 dpf, mCherry^{+} interstitial fibroblasts in the trunk were largely GFP^{-}, suggesting
279 the absence of active BMP signaling (Fig 6E). By contrast, cells at the periphery showed different
280 levels of BMP signaling: stromal reticular cells were weakly positive for *BRE:GFP*, while ventral fin
281 mesenchymal cells displayed strong BMP response (Fig 6E). Consistent with this result, *nkx3.1*$^{NTR\text{-}}$
282 ^{mCherry}-positive fin mesenchymal cells showed elevated level of phospho-Smad (pSmad), a sensitive
283 readout of BMP signaling (Fig 6F). Together, our results suggest that local BMP ligands from apical
284 epidermal cells activate robust BMP response in fin mesenchymal cells.
285
286 **Development of fin mesenchymal cells is regulated by BMP signaling**
287 Since fin mesenchymal cells show strong BMP signaling compared to other sclerotome derived
288 cells, we hypothesized that active BMP signaling is required for the proper development of fin
289 mesenchymal cells. To test this possibility, we utilized DMH1, a specific BMP receptor inhibitor (Hao
290 et al., 2010), to block BMP signaling. Treatment of *BRE:GFP* fish with DMH1 from 10 to 24 hpf
291 substantially reduced the GFP expression (Fig S3), confirming DMH1 as an effective inhibitor of BMP
292 signaling. To examine whether BMP signaling regulates fin mesenchymal cell development, we
293 treated *kdrl:EGFP; nkx3.1*$^{NTR\text{-}mCherry}$ embryos with DMH1 from 18 hpf (prior to the migration of
294 sclerotome derived cells) to 48 hpf. Similar to what has been described (Wiley et al., 2011), DMH1-
295 treated fish showed poorly formed CVP, a structure dependent on active BMP signaling (Fig 7A).
296 Strikingly, DMH1 treatment resulted in an obvious expansion of the fin fold, accompanied by a
297 substantial reduction of mCherry^{+} fin mesenchymal cells in both the dorsal and ventral fin folds (Fig
298 7A). Quantification of the height of the fin fold showed 51% (dorsal fin) and 39% (ventral fin)
299 expansion in DMH1-treated fish (Fig 7B). By contrast, quantification of a 10-somite region showed
300 that inhibition of BMP signaling lead to 49% reduction of dorsal fin mesenchymal cells (from 54.2 to
301 27.7), and 63% decrease in ventral fin mesenchymal cells (from 39.8 to 14.6) (Fig 7C). Interestingly,
302 the few remaining fin mesenchymal cells in DMH1-treated fish showed an aberrant cell morphology
303 with more cellular projections compared to controls (Fig 7A). To determine whether BMP signaling

304 regulates the branching morphogenesis of fin mesenchymal cells, we performed late DMH1
305 treatments on *kdrl:EGFP; nkx3.1*$^{NTR\text{-}mCherry}$ embryos at 25-49 hpf (Fig S4). Similar to early DMH1
306 treatment, fin folds in DMH1-treated embryos were significantly expanded (Fig S4A and S4B).
307 Although the number of fin mesenchymal cells was largely unaffected in DMH1-treated fish (Fig S4C),
308 they displayed the similar hyperbranching morphology (Fig S4A). Our results suggest that BMP
309 signaling is required in not only the early migration but also the late morphogenesis of fin
310 mesenchymal cells. To further characterize the regulation of fin development by BMP signaling, we
311 analyzed different fin markers in embryos treated with DMH1 at 18-45.5 hpf. As expected, DMH1
312 treatment resulted in reduced *fbln1* expression in fin mesenchymal cells, but lead to a substantial
313 expansion of apical epidermal cells marked by *bmp4* and *fras1* expression (Fig 7D). This result
314 suggests that the inhibition of BMP signaling compromises the development of fin mesenchymal cells,
315 and the expansion of apical epidermal cells leads to the overgrowth phenotype of the fin fold.
316 Together, our results suggest that local BMP signaling in the fin fold is required for the migration and
317 morphogenesis of fin mesenchymal cells.

318 **DISCUSSION**

319

320 Our work establishes the sclerotome as a new system to explore cell fate diversification in
321 embryonic development. Three major conclusions can be drawn from our studies. First, the
322 sclerotome is the embryonic source of distinct tissue-resident fibroblasts. Second, sclerotome
323 progenitors are multipotent, and their differentiation is determined by their axial positions and
324 migratory paths. Third, development of fin mesenchymal cells from sclerotome progenitors requires
325 local BMP signals in the fin fold. Together, our work suggests that the local microenvironment
326 contributes to the diversification of fibroblast subtypes from multipotent sclerotome progenitors during
327 embryonic development.

328

329 **The sclerotome is the embryonic source of tissue-resident fibroblasts**

330 The embryonic sclerotome is known to give rise to the axial skeleton, including the bones and
331 cartilage of the body. Our previous studies (Ma et al., 2018; Rajan et al., 2020) and our current work
332 provide strong evidence that the sclerotome is the embryonic source of multiple types of fibroblast
333 populations in the trunk. Sclerotome derived fibroblasts share the expression of the pan-fibroblast
334 marker *col1a2*, and likely provide structural support to a variety of tissues. Based on their marker
335 expression, cell location and morphology, we identify at least four fibroblast subtypes: tenocytes, fin
336 mesenchymal cells, blood vessel associated fibroblasts, and interstitial fibroblasts. Tenocytes express
337 classic tendon markers *scxa* and *tnmd* (Chen and Galloway, 2014; Ma et al., 2018). Their cell bodies
338 are positioned medially along the myotendinous junction while extending long cellular processes into
339 the intersomitic space (Ma et al., 2018). Tenocytes function to stabilize muscle attachment, likely by
340 secreting a number of ECM proteins (Ma et al., 2018; Subramanian and Schilling, 2014). Fin
341 mesenchymal cells, on the other hand, are marked by the expression of ECM genes *hmcn2* and *fbln1*.
342 They are located adjacent to apical epidermal cells in the fin fold, extending tree-like processes
343 distally. Recent work has shown that fin mesenchymal cells guide fin formation by aligning collagen
344 fibers of actinotrichia (Kuroda et al., 2020). Genetic ablation of fin mesenchymal cells in the pectoral
345 and median fin folds results in a collapse of the respective fins (Lalonde and Akimenko, 2018). By
346 contrast, although blood vessel associated fibroblasts are closely associated with the vasculature,
347 their morphologies differ depending on the vascular bed. For example, ISV-associated perivascular
348 fibroblasts are more globular, whereas DLAV fibroblasts are more elongated. We have previously
349 shown that perivascular fibroblasts play dual roles in stabilizing nascent ISVs as well as functioning as
350 pericyte precursors (Rajan et al., 2020). It is likely that other blood vessel associated fibroblasts play
351 similar roles in stabilizing the corresponding blood vessels. Interestingly, stromal reticular cells closely

352 interact with the CVP, which functions as the early hematopoietic niche during development (Wattrus
353 and Zon, 2018). Indeed, recent work has shown that defects in SRC maturation result in a
354 compromised CVP niche that fails to support hematopoietic stem cell (HSC) maintenance and
355 expansion (Murayama et al., 2015). Therefore, SRCs might not only provide the structural support to
356 the CVP but also modulate the microenvironment required for HSC differentiation. Compared to other
357 fibroblast subtypes, interstitial fibroblasts are the least well characterized. Based on their distribution
358 around the notochord and the spinal cord, it is conceivable that interstitial fibroblasts give rise to
359 osteoblasts required for the vertebral column development. Together, our results suggest that the
360 sclerotome generates distinct fibroblast subtypes to support a variety of tissues, including muscles,
361 fins and blood vessels.
362
363 **The developmental origin of fin mesenchymal cells**
364 There has been considerable debate as to where fin mesenchymal cells originate from during fish
365 and amphibian development. Lineage tracing studies in zebrafish suggest that the paraxial
366 mesoderm, specifically the dermomyotome, is the embryonic source of fin mesenchymal cells (Lee et
367 al., 2013), which contrasts with our findings. To rule out sclerotome contribution, Lee et al. (2013) use
368 the *ola-twist1:Gal4* transgenic line, in which Gal4 expression is driven by the medaka (*Oryzias latipes*)
369 *twist1* promoter. Interestingly, we have previously shown that the expression of a similar *ola-*
370 *twist1:EGFP* reporter is restricted to sclerotome derived cells around the notochord, but absent in both
371 dorsal and ventral sclerotome domains (Ma et al., 2018). This observation explains why the *ola-*
372 *twist1:Gal4* line fails to label any fin mesenchymal cells (Lee et al., 2013). Interestingly, our results
373 show that the sclerotome only contributes to fin mesenchymal cells in the dorsal and ventral portion of
374 the major lobe of the fin fold. No sclerotome contribution to the minor lobe or the caudal tail fin in the
375 major lobe could be observed. Combining with previous work (Lee et al., 2013), it is likely that fin
376 mesenchymal cells are generated by multiple different lineages depending on their locations. Fin
377 mesenchymal cells in the dorsal and ventral fin fold are of sclerotome origin, those in the tail fin
378 originate from the dermomyotome, while fin mesenchymal cells in the minor lobe of the fin fold have
379 an unidentified embryonic source.
380
381 **Multipotent sclerotome progenitors are fated by local signals**
382 One fundamental question in development biology is how distinct cell types are differentiated from
383 a single progenitor cell. To explore this question, we used *nkx3.1*-based transgenic reporters to
384 analyze the lineage diversification from the sclerotome. Photoconversion-based clonal analysis
385 reveals that single sclerotome progenitors are capable of generating 2-3 distinct fibroblast subtypes.

386 This result suggests that individual sclerotome progenitors are likely multipotent, rather than "lineage-
387 restricted" to differentiate into one specific fibroblast subtype. Our studies reveal three key features in
388 cell fate diversification of sclerotome progenitors (Fig 7E). First, sclerotome progenitors display
389 regional differences in their differentiation potential along the dorsal-ventral and anterior-posterior
390 positions. Dorsally located fibroblasts, such as dorsal fin mesenchymal cells and DLAV fibroblasts,
391 are derived from the dorsal sclerotome, while ventrally located fibroblasts, such as stromal reticular
392 cells and ventral fin mesenchymal cells, are generated by the ventral sclerotome. Similarly, the ventral
393 sclerotome in anterior somites (before the end of the yolk extension) generates only fibroblasts in the
394 trunk, whereas the ventral sclerotome in posterior somites contributes to the SRC and fin
395 mesenchymal cell populations in addition to fibroblasts in the trunk. Second, fates of sclerotome
396 progenitors are biased by their migratory path. For dorsal sclerotome progenitors, dorsal migration
397 limits the cell to become either dorsal fin mesenchymal cells or DLAV fibroblasts, while ventral
398 migration leads to the differentiation of predominately tenocytes or perivascular fibroblasts. Third, the
399 relative order of migrating sclerotome progenitors largely determines their differentiation potential.
400 Leading cells are more likely to become ventral fin mesenchymal cells, while lagging cells tend to
401 differentiate into SRCs. The combination of these three mechanisms results in the generation of
402 different fibroblast subtypes in a stereotypic manner (Ma et al., 2018; Rajan et al., 2020).
403 How does a sclerotome progenitor decide which cell type to differentiate into? Analysis of the fin
404 fold strongly suggests that local microenvironment plays an instructive role in cell fate diversification.
405 In the fin fold, a number of BMP ligands, including *bmp2b*, *bmp4*, and *bmp6*, are expressed distally in
406 apical epidermal cells. Due to the proximity to the BMP source, leading cells of migrating sclerotome
407 progenitors are exposed to likely the highest level of BMP ligands. This is consistent with stronger
408 BMP response in fin mesenchymal cells compared to stromal reticular cells, mostly generated by
409 lagging cells. Therefore, different levels of BMP signaling might guide the migration and maturation of
410 different sclerotome derived cells. Indeed, inhibition of BMP signaling by DMH1 greatly reduces the
411 number of fin mesenchymal cells, suggesting that BMP signaling is required for the development of fin
412 mesenchymal cells. The role of BMP signaling in fin mesenchymal cell development at the periphery
413 mirrors the dependence of Hh signaling in tenocyte specification in the trunk (Ma et al., 2018),
414 suggesting that local cell signaling pathways contribute to the differentiation of sclerotome
415 progenitors. Taken together, our work on the sclerotome lineage suggests a model where local
416 microenvironment determines the fate of sclerotome progenitors. The cell type diversification of the
417 sclerotome lineage is remarkably similar to the neural crest lineage. Previous studies have shown that
418 migrating neural crest cells are multipotent (Baggiolini et al., 2015), and the ultimate cell fates are
419 determined by their axial positions, as well as the migration timing and direction (Rocha et al., 2020).

420

421 **BMP signaling plays dual roles in fin fold development**

422 The zebrafish fin fold is comprised of two juxtaposing cell layers: the proximal layer of fin
423 mesenchymal cells and the distal layer of apical epidermal cells. Our studies reveal that BMP
424 signaling regulates the development of both cell populations. First, BMP signaling is essential for the
425 migration and specification of fin mesenchymal cells. This is likely mediated by paracrine BMP
426 signaling from BMP-expressing apical epidermal cells to BMP-responding fin mesenchymal cells.
427 Inhibition of BMP signaling results in a substantial reduction in the number of fin mesenchymal cells,
428 and the few remaining cells often display an aberrant hyperbranching morphology. This result
429 suggests that BMP signaling is required not only for the migration of fin mesenchymal cell precursors
430 into the fin fold, but also their morphogenesis once they reach the destination. BMP signaling has
431 been previously implicated in the regulation of cell migration in other in vivo contexts, including the
432 migration of neural crest cells (Fu et al., 2006; Goldstein et al., 2005; Sela-Donenfeld and Kalcheim,
433 1999) and cortical neurons (Saxena et al., 2018). Interestingly, despite the loss of fin mesenchymal
434 cells, blockage of BMP signaling results in a significant outgrowth of the fin fold. This phenotype is
435 likely caused by the expansion of apical epidermal cells. Therefore, BMP signaling plays a second
436 role in restricting the outgrowth of apical epidermal cells. A recent study suggests that the fin fold
437 expansion upon BMP inhibition is likely caused by prolonged cell proliferation, altered cell division
438 orientation as well as excessive distal cell migration in the fin fold (Ka et al., 2020). Although our
439 results strongly argue that BMP signaling is required autonomously in fin mesenchymal cells for its
440 normal development, we cannot rule out the possibility that the altered ECM environment due to the
441 expansion of apical epidermal cells contributes to certain aspects of the phenotype as previously
442 suggested (Feitosa et al., 2012). Together, our results suggest a model where BMP signaling
443 regulates the recruitment and morphogenesis of fin mesenchymal cells while controlling the size of
444 the fin fold. Interestingly, fin mesenchyme migration defects have been previously proposed as a
445 potential mechanism underlying the fin-to-limb transition during evolution (Nakamura et al., 2016;
446 Zhang et al., 2010). Our findings raise the possibility that the re-wiring of BMP signaling might
447 contribute to the evolution of tetrapod digits.

448

449

450 In summary, we demonstrate that the sclerotome is the embryonic source of multiple fibroblast
451 populations in zebrafish. Our work shows that the sclerotome is an excellent model to study cell type
452 diversification during embryonic development. The combination of positional and migratory
453 information as well as local microenvironment likely determines the differentiation trajectory of

454 multipotent sclerotome progenitors. Although our work highlights the importance of extrinsic cues, cell
455 intrinsic programs likely also contribute to the cell fate diversification. Future work using single cell
456 RNA sequencing will likely identify key gene regulatory networks underlying the lineage progression of
457 sclerotome progenitors.

458 **MATERIALS AND METHODS**

459

460 **Ethics statement**

461 All animal research was conducted in accordance with the principles outlined in the current
462 Guidelines of the Canadian Council on Animal Care. All protocols were approved by the Animal Care
463 Committee at the University of Calgary (#AC17-0128).

464

465 **Zebrafish strains**

466 Zebrafish strains used in this study were maintained and raised under standard conditions. The
467 following transgenic strains were used in this study: *Tg(BRE:GFP)mw29* (Collery and Link, 2011),
468 *TgBAC(col1a2:Gal4)ca102* (Ma et al., 2018; Sharma et al., 2019), *TgBAC(col1a2:GFP)ca103* (Ma et
469 al., 2018), *Tg(kdrl:EGFP)la163* (Choi et al., 2007), *TgBAC(nkx3.1:Gal4)ca101* (Ma et al., 2018),
470 *Tg(UAS:Kaede)s1999t* (Davison et al., 2007), and *Tg(UAS:NTR-mCherry)c264* (Davison et al., 2007).
471 The mosaic *col1a2:Gal4; UAS:Kaede* line was maintained by screening for embryos with more
472 mosaic Kaede expression.

473

474 **In situ hybridization and immunohistochemistry**

475 Whole-mount in situ hybridization and immunohistochemistry were performed according to
476 previously established protocols. We used the following RNA probes in this study: *bmp2b*, *bmp4*,
477 *bmp6*, *hmcn2*, *fbln1*, and *fras1*. Double fluorescent in situ hybridizations were performed using
478 different combinations of digoxigenin (DIG) or dinitrophenyl (DNP) labeled probes. For
479 immunohistochemistry, rabbit polyclonal antibody to RFP (1:1000, MBL, PM005) and rabbit polyclonal
480 antibody to phosphoSmad 1/5/9 (1:100, Cell Signaling Technology, 13820) were used. For fluorescent
481 detection of antibody labeling, the appropriate Alexa Fluor-568 or Alexa Fluor-647 secondary
482 antibodies (1:500, Thermo Fisher) was used.

483

484 **Kaede photoconversion**

485 Photoconversion was carried out using the 405nm laser and the 20x objective on the Olympus
486 FV1200 confocal microscope. At the appropriate stage, Kaede-expressing embryos were
487 anesthetized using tricaine and mounted in 0.8% low melting point agarose. The duration and
488 intensity of laser required for complete green-to-red conversion depended on the expression level of
489 Kaede and the size of the target region. For cell tracing of the sclerotome domains, typically a circular
490 region of 20 by 20 pixels was converted using 1.5% 405nm laser for 4 seconds. For single cell clonal
491 analysis of sclerotome progenitors, typically a circular region of 10 by 10 pixels was converted using

492 1.5% 405nm laser for 4 seconds. After photoconversion, embryos were confirmed for expression of
493 Kaede^{red} and recovered in E3 fish water until necessary stages.
494
495 **Time-lapse imaging and cell tracking**
496 Time-lapse imaging of zebrafish embryos was carried out using the Olympus FV1200 confocal
497 microscope. At the appropriate stage, fish were anesthetized using tricaine and mounted in 0.8% low
498 melting point agarose. To keep the agarose hydrated and minimize the development of pigments as
499 well as minimize movement of the fish, a small volume of E3 water with phenylthiourea and tricaine
500 was carefully flooded around the agarose. Z-stack images of the region of interest were then collected
501 at regular intervals (6-9 mins) for up to 25 hours. Images were then compiled into movies using the
502 Olympus Fluoview software. Cells from each movie were then manually tracked using Fiji (Schindelin
503 et al., 2012).
504
505 **Drug treatments**
506 Embryos at the appropriate stage were treated in DMH1 (Sigma Millipore, D8696) at a final
507 concentration of 10 μM in E3 fish water. Control embryos were treated similarly in an equal
508 concentration of DMSO. Treated embryos were grown to the desired stage for analysis.
509
510 **Statistical analysis**
511 All the graphs were generated in the GraphPad Prism software. Data were plotted as mean ±
512 SEM. Significance between two samples was calculated using Mann-Whitney *U* test. p values: $p > 0.05$
513 (not significant); $p < 0.05$ (*); $p < 0.01$ (**); $p < 0.001$ (***); $p < 0.0001$ (****).

ACKNOWLEDGMENTS

We thank the zebrafish community for providing probes and reagents; Sarah Childs for sharing reagents, transgenic lines and providing critical input on this project; members of the Childs and Huang laboratories for discussions; Arsheen Rajan and Emilio Méndez Olivos for critical comments on the manuscript.

COMPETING INTERESTS

The authors declare that no competing interests exist.

FUNDING

This study was supported by grants to P.H. from the Canadian Institute of Health Research (MOP-136926 and PJT-169113), Canada Foundation for Innovation John R. Evans Leaders Fund (Project 32920), and Startup Fund from the Alberta Children's Hospital Research Institute (ACHRI).

534 **FIGURE LEGENDS**

535

536 **Fig 1. Characterization of sclerotome derived fibroblasts.** (A) Schematic representation of
537 sclerotome derived fibroblasts. Four major cell types are shown: blood vessel associated fibroblasts,
538 fin mesenchymal cells, tenocytes, and interstitial fibroblasts. Each cell type is defined by its location in
539 the trunk and its cell morphology. Lateral view of 2 somites is shown with the major blood vessels
540 (green) indicated (DLAV: dorsal longitudinal anastomotic vessel; ISV: intersegmental vessel; DA:
541 dorsal aorta; CVP: caudal vein plexus). n: notochord. (B) The *nkx3.1*$^{NTR\text{-}mCherry}$ line (red) was crossed
542 to the *kdrl:EGFP* line (green) to label the endothelial cells. At 2 dpf, mCherry^{+} cells were seen
543 populated throughout the zebrafish trunk (top panels). Zoomed in views (bottom panels) show
544 different mCherry^{+} fibroblast subtypes (arrows) in 4 boxed regions in the trunk. mCherry expression in
545 some muscles and skin cells at the edge of the fin fold are denoted by asterisks and arrowheads,
546 respectively. *n* = 13 embryos. (C) The mosaic *col1a2*^{Kaede} line (green) was crossed to the *kdrl:mCherry*
547 line (red). High resolution images showed that individual blood vessel associated fibroblasts (cyan
548 arrows), fin mesenchymal cells (white arrows), tenocytes (magenta arrow), and interstitial fibroblasts
549 (yellow arrow) displayed distinct morphologies. The corresponding vascular bed is indicated for blood
550 vessel associated fibroblasts. The corresponding fin fold is indicated for fin mesenchymal cells. Cell
551 processes are indicated by arrowheads. *n* = 20 embryos. Scale bars: (B) 50 µm; (C) 20 µm.

552

553 **Fig 2. Lineage analysis of sclerotome domains.** (A) Schematic representation of lineage analysis.
554 The entire dorsal or ventral sclerotome domain in *nkx3.1*^{Kaede} embryos were labeled by
555 photoconversion at 24 hpf. The lineage of the converted cells was then imaged after 24 hours and
556 analyzed for the cell types that were generated. (B) Photoconversion of the dorsal sclerotome domain
557 in *nkx3.1*^{Kaede} embryos. Images of two examples are shown right after the conversion at 24 hpf and 24
558 hours later at 48 hpf. Cell projections at 24 hpf are denoted by white arrowheads. The dorsal
559 sclerotome domain gave rise to dorsal fin mesenchymal cells (white arrows), DLAV fibroblasts (long
560 cyan arrows), perivascular fibroblasts (cyan arrows), tenocyte (magenta arrows), and interstitial
561 fibroblasts (yellow arrows). The outline of the vasculature is denoted by dotted lines. *n* = 20 embryos.
562 (C) Photoconversion of the ventral sclerotome domain in *nkx3.1*^{Kaede} embryos. Images of two
563 examples are shown at 24 hpf and 48 hpf. In anterior somites above the yolk extension (upper panel),
564 the ventral sclerotome domain gave rise to perivascular fibroblasts (cyan arrows), tenocytes (magenta
565 arrows), and interstitial fibroblasts (yellow arrows), but not SRCs or ventral fin mesenchymal cells. In
566 posterior somites above the CVP region (bottom panel), the ventral sclerotome domain gave rise to
567 SRCs (cyan arrowheads) and ventral fin mesenchymal cells (white arrows) in addition to tenocytes

568 (magenta arrows) and interstitial fibroblasts (yellow arrows) in the trunk. The ventral boundary of the
569 CVP is indicated by dotted lines. *n* = 20 embryos. Asterisks in (B, C) denote pigment cells that show
570 strong autofluorescence in the red channel. Scale bars: 50 µm.
571
572 **Fig 3. Single cell lineage analysis of the dorsal sclerotome domain.** (A) Schematic representation
573 of lineage tracing experiment. A single dorsal sclerotome progenitor in *nkx3.1*^{Kaede} embryos was
574 photoconverted at 24 hpf and imaged after 24 hours to determine the cell types generated. Dorsal
575 sclerotome derived cells at 48 hpf were subdivided into two groups based on their dorsal-ventral
576 positions: the more dorsal type I cells include dorsal fin mesenchymal cells and DLAV fibroblasts
577 (above the dotted line), while the more ventral type II cells include tenocytes, perivascular fibroblasts,
578 and interstitial fibroblasts (below the dotted line). (B) Quantification of the cell number in each clone.
579 (C) Quantification of the number of fibroblast subtypes in each clone. (D) Distribution of different
580 fibroblast subtypes from all decedents of traced cells. F: dorsal fin mesenchymal cells; T: tenocytes;
581 V: blood vessel associated fibroblasts; I: interstitial fibroblasts. (E) Quantification of the types of cells
582 generated by individually labeled dorsal sclerotome progenitors. Only photoconverted cells showing
583 polarized cell projections at 24 hpf were graphed. *n* = 14 (with dorsal projection) and 19 (with ventral
584 projection) photoconverted cells. (F) Photoconversion of a single dorsal sclerotome cell in *nkx3.1*^{Kaede}
585 embryos. Two examples are shown at 24 hpf and 48 hpf. In the top panel (type I cell lineage), the
586 photoconverted cell showing dorsal projections (arrowhead) gave rise to two dorsal fin mesenchymal
587 cells (white arrows) and a DLAV fibroblasts (long cyan arrows). In the bottom panel (type II cell
588 lineage), the photoconverted cell with ventral cell projections (arrowhead) gave rise to one DLAV
589 fibroblasts (long cyan arrows), one perivascular fibroblast (cyan arrows) and one tenocyte (magenta
590 arrows). The outline of the vasculature is denoted by dotted lines. *n* = 42 photoconverted cells traced
591 from 40 embryos. Scale bars: 50 µm.
592
593 **Fig 4. Time-lapse imaging of the migration of ventral sclerotome progenitors.** Snapshots of a
594 *kdrl:EGFP; nkx3.1*$^{NTR\text{-}mCherry}$ embryo between 25 hpf and 50 hpf are shown with time stamps (hh:mm)
595 indicated. Cell migration and divisions of representative lagging (cyan arrows) and leading (white
596 arrows) cells were traced throughout their migration. The lagging cell never migrated ahead of the
597 leading cell and generated 2 SRCs. The leading cell remained at the migration front ahead of the
598 lagging cell and generated 2 ventral fin mesenchymal cells. *n* = 7 embryos. Scale bar: 50 µm.
599
600 **Fig 5. Single cell lineage analysis of the ventral sclerotome domain.** (A) Schematic
601 representation of lineage tracing experiment. A single ventral sclerotome progenitor in *nkx3.1*^{Kaede}

602 embryos was photoconverted at 24 hpf and imaged after 24 hours to determine the cell types
603 generated. Cells were classified into lagging or leading cells based on its initial position at 24 hpf.
604 Leading cells were defined at the front of the migration path, while lagging cells were defined as any
605 cell behind the leading cell. (B) Quantification of the types of cells generated by lagging and leading
606 cells. (C) Examples of a photoconverted lagging cell (top panel) and a photoconverted leading cell
607 (bottom panel) are shown at 24 hpf and 48 hpf. The lagging cell generated 4 SRCs (cyan arrowheads)
608 and all photoconverted cells remained dorsal to the ventral edge of the CVP (dotted lines). The
609 photoconverted leading cell migrated ahead of the CVP and generated 2 fin mesenchymal cells (white
610 arrows). *n* = 42 photoconverted cells traced from 38 embryos. Scale bars: 50 µm.
611
612 **Fig 6. Sclerotome derived fin mesenchymal cells are active in BMP signaling.** (A) Schematic
613 representation of the organization of the zebrafish fin fold. Both dorsal and ventral fin folds are
614 populated by two adjacent cell layers: a distal layer of apical epidermal cells, and a proximal layer of
615 fin mesenchymal cells. (B) Double fluorescent in situ staining of *fbln1* (red) with *fras1* or *hmcn2*
616 (green) at 48 hpf. *fras1* labeled the distal apical epidermal cell layer (orange brackets), *fbln1* marked
617 the proximal layer of fin mesenchymal cells (white brackets), while *hmcn2* was expressed in both
618 layers. *n* = 15 embryos per staining. (C) *nkx3.1*$^{NTR\text{-}mCherry}$ embryos were co-stained with *fbln1*, *fras1*, or
619 *bmp4* probes (green) and anti-mCherry antibody (red) at 52 hpf. Apical epidermal cells and fin
620 mesenchymal cells are indicated by arrowheads and arrows, respectively. *bmp4* was expressed in
621 *fras1*$^{+}$ apical epidermal cells adjacent to mCherry^{+} *fbln1*$^{+}$ fin mesenchymal cells. *n* = 10 embryos per
622 staining. (D) Double fluorescent in situ staining of *bmp4* (green) with *fbln1* or *fras1* (red) at 48 hpf.
623 *bmp4* was expressed in *fras1*$^{+}$ apical epidermal cells (orange brackets) adjacent to *fbln1*$^{+}$ fin
624 mesenchymal cells (white brackets). Asterisks denote *bmp4* expression in the dorsal spinal cord. *n* =
625 15 embryos per staining. (E) *nkx3.1*$^{NTR\text{-}mCherry}$ fish were crossed to *BRE:GFP* to label BMP responsive
626 cells. At 2 dpf, mCherry^{+} fin mesenchymal cells (white arrows) and SRCs (cyan arrows) were marked
627 by strong and weak GFP expression, respectively. In contrast, no GFP expression was found in
628 mCherry^{+} interstitial fibroblasts (yellow arrows) around the notochord (nc). *n* = 9 embryos. (F)
629 *kdrl:EGFP; nkx3.1*$^{NTR\text{-}mCherry}$ embryos were stained with pSmad antibody (cyan) at 2 dpf. mCherry^{+} fin
630 mesenchymal cells showed elevated pSmad staining (arrows). *n* = 14 embryos. Magnified views of
631 boxed regions in (B, D, F) are shown in corresponding panels. Scale bars: (B, D, E, F) 50 µm; (C) 20
632 µm.
633
634 **Fig 7. Regulation of fin mesenchymal cells by BMP signaling.** (A) *kdrl:EGFP; nkx3.1*$^{NTR\text{-}mCherry}$
635 embryos were treated with either DMSO or DMH1 between 18 hpf and 48 hpf. DMH1 treatment

636 resulted in the expansion of both dorsal and ventral fin folds (brackets), poorly developed CVP
637 (asterisk), and the reduction of mCherry^{+} fin mesenchymal cells in both the dorsal and ventral fin folds
638 (arrows). Remaining fin mesenchymal cells in DMH1-treated embryos appeared to have more
639 branches (arrowheads) compared to DMSO-treated controls in magnified views. n = 19 embryos per
640 condition. (B) Quantification of the fin fold expansion in DMH1 treated embryos. The heights of the
641 dorsal fin fold, ventral fin fold, and somite were measured at somite 26. Fin fold height was normalized
642 to the height of the somite of the same embryo. n = 11 (DMSO) and 9 (DMH1) embryos. (C)
643 Quantification of the number of fin mesenchymal cells in DMH1 treated fish. Fin mesenchymal cells
644 were counted in either the dorsal or ventral fin fold between somites 18 and 28. Each point represents
645 the total number of fin mesenchymal cells in 10 somite region of one fish. n = 11 (DMSO) and 10
646 (DMH1) embryos. Data in (B, C) are plotted as mean ± SEM. Statistics: Mann-Whitney U test; $p <$
647 0.01 (**); $p < 0.001$ (***). (D) Wild-type embryos were treated with DMSO or DMH1 from 18 hpf to 45.5
648 hpf and stained with *fbln1*, *bmp4*, and *fras1* probes. *fbln1* expression was markedly reduced in both
649 the dorsal and ventral fin folds (arrowheads and arrows, respectively), while *bmp4* and *fras1*
650 expression was expanded along the fin fold compared to DMSO controls. The anterior extent of *fbln1*
651 expression in the dorsal fin fold is denoted by asterisks. n = 15 embryos per condition. (E) Model of
652 diversification of fibroblast subtypes from sclerotome progenitors in zebrafish. Three mechanisms
653 contribute to the diversification of fibroblast subtypes from multipotent sclerotome progenitors. a)
654 Spatial regulation. Sclerotome progenitors at the different dorsal-ventral or anterior-posterior positions
655 have distinct differentiation potentials. b) Migration direction. The fates of sclerotome progenitors are
656 biased by the direction of their migration. c) Migration order. The fates of sclerotome progenitors are
657 determined by their position along the migratory path. Local microenvironment (for example, BMP
658 expression (indicated by the blue band) at the periphery of the fin fold) regulates the migration,
659 specification and morphogenesis of fin mesenchymal cells. n: notochord; CVP: caudal vein plexus.
660 Scale bars: (A) 50 µm (20 µm for magnified views); (D) 200 µm.

661 **SUPPLEMENTAL FIGURES**

662

663 **Fig S1. The sclerotome generates a population of fibroblasts.** (A) Wild-type embryo at 2 dpf. The
664 major lobe and minor lobe of the fin fold are outlined by dash lines. (B) A tiled confocal image of
665 *nkx3.1*$^{NTR\text{-}mCherry}$ embryo at 2 dpf showing mCherry^{+} sclerotome derived cells (red) throughout the
666 trunk of the embryo. mCherry^{+} fin mesenchymal cells were present in both dorsal and ventral fin fold
667 (arrows), but absent from the caudal fin and the minor lobe (asterisks). Arrowhead indicates mCherry
668 expression in skin cells at the edge of the fin fold. (C) The *nkx3.1*$^{NTR\text{-}mCherry}$ line (red) was crossed to
669 the *col1a2:GFP* line (green). At 2 dpf, most mCherry^{+} sclerotome derived cells also expressed
670 *col1a2:GFP*. The upper panel shows dorsal fin mesenchymal cells (white arrows), DLAV fibroblasts
671 (long cyan arrows), ISV-associated perivascular fibroblasts (cyan arrows), tenocytes (magenta
672 arrows), and interstitial fibroblasts (yellow arrows) in the dorsal region of the trunk. The middle panel
673 shows DA fibroblasts (cyan arrows) associated with the dorsal aorta. The bottom panel shows stromal
674 reticular cells (cyan arrows) and ventral fin mesenchymal cells (white arrows). *n* = 12 embryos. Scale
675 bars: (A-B) 200 µm; (C) 50 µm.

676

677 **Fig S2. Apical epidermal cells express BMP ligands.** (A) Double fluorescent in situ staining of
678 *bmp4* (green) with *hmcn2* (red) at 48 hpf. (B) Double fluorescent in situ staining of *bmp2b* (green) with
679 *fbln1* or *fras1* (red) at 48 hpf. (C) Double fluorescent in situ staining of *bmp6* (green) with *fbln1* or *fras1*
680 (red) at 48 hpf. *bmp4*, *bmp2b*, and *bmp6* were expressed in *hmcn2*$^{+}$*fras1*$^{+}$ apical epidermal cells
681 (orange brackets) adjacent to *hmcn2*$^{+}$*fbln1*$^{+}$ fin mesenchymal cells (white brackets). Magnified views
682 of boxed regions are shown in each staining. *n* = 15 embryos per staining. Scale bars: 50 µm.

683

684 **Fig S3. Effective inhibition of BMP signaling by DMH1.** *BRE:GFP* embryos were treated with
685 either DMSO or DMH1 between 10 hpf and 24 hpf and imaged for GFP expression. GFP expression
686 was substantially reduced in the trunk of DMH1 treated embryos (arrows). *n* = 10 embryos per
687 condition. Scale bar: 50 µm.

688

689 **Fig S4. BMP signaling regulates the morphogenesis of fin mesenchymal cells.** (A) *kdrl:EGFP;*
690 *nkx3.1*$^{NTR\text{-}mCherry}$ embryos were treated with either DMSO or DMH1 between 25 hpf and 49 hpf. DMH1
691 treatment resulted in the expansion of both dorsal and ventral fin folds (brackets). Fin mesenchymal
692 cells (arrows) in DMH1-treated embryos appeared to have more branches (arrowheads) compared to
693 DMSO-treated controls in magnified views of boxed regions. *n* = 13 (DMSO) and 14 (DMH1) embryos.
694 (B) Quantification of the fin fold expansion in DMH1 treated embryos. The heights of the dorsal fin

695 fold, ventral fin fold, and somite were measured at somite 23. Fin fold height was normalized to the
696 height of the somite of the same embryo. (C) Quantification of the number of fin mesenchymal cells in
697 DMH1 treated fish. Fin mesenchymal cells were counted in either the dorsal or ventral fin fold
698 between somites 18 and 28. Each point represents the total number of fin mesenchymal cells in 10
699 somite region of one fish. Data are plotted as mean ± SEM. Statistics: Mann-Whitney *U* test; $p > 0.05$
700 (ns, not significant); $p < 0.001$ (***); $p < 0.0001$ (****). Scale bars: 50 µm.
701
702 **Video S1. Time-lapse imaging of the migration of ventral sclerotome progenitors.** *kdrl:EGFP;*
703 *nkx3.1*$^{NTR\text{-}mCherry}$ embryos were imaged from 25 hpf to 50 hpf with time stamps (hh:mm) indicated. Cell
704 migration and divisions of representative lagging (cyan arrows) and leading (white arrows) cells were
705 traced throughout their migration. Daughter cells are indicated by arrows of the same color. The
706 lagging cell never migrated ahead of the leading cell and generated 2 SRCs. The leading cell
707 remained at the migration front ahead of the lagging cell and generated 2 ventral fin mesenchymal
708 cells. Snapshots of this video are shown in Fig 4. $n = 7$ embryos. Scale bar: 50 µm.
709

710 **REFERENCES**

711

712 Baggiolini, A., Varum, S., Mateos, J.M., Bettosini, D., John, N., Bonalli, M., Ziegler, U., Dimou, L.,
713 Clevers, H., Furrer, R., et al. (2015). Premigratory and migratory neural crest cells are multipotent in
714 vivo. Cell Stem Cell *16*, 314–322.

715 Brent, A.E., Schweitzer, R., and Tabin, C.J. (2003). A somitic compartment of tendon progenitors. Cell
716 *113*, 235–248.

717 Carney, T.J., Feitosa, N.M., Sonntag, C., Slanchev, K., Kluger, J., Kiyozumi, D., Gebauer, J.M.,
718 Talbot, J.C., Kimmel, C.B., Sekiguchi, K., et al. (2010). Genetic analysis of fin development in
719 zebrafish identifies furin and Hemicentin1 as potential novel fraser syndrome disease genes. PLoS
720 Genetics *6*.

721 Chen, J.W., and Galloway, J.L. (2014). The development of zebrafish tendon and ligament
722 progenitors. Development (Cambridge, England) *141*, 2035–2045.

723 Choi, J., Dong, L., Ahn, J., Dao, D., Hammerschmidt, M., and Chen, J.N. (2007). FoxH1 negatively
724 modulates flk1 gene expression and vascular formation in zebrafish. Developmental Biology *304*,
725 735–744.

726 Collery, R.F., and Link, B.A. (2011). Dynamic smad-mediated BMP signaling revealed through
727 transgenic zebrafish. Developmental Dynamics *240*, 712–722.

728 Davison, J.M., Akitake, C.M., Goll, M.G., Rhee, J.M., Gosse, N., Baier, H., Halpern, M.E., Leach,
729 S.D., and Parsons, M.J. (2007). Transactivation from Gal4-VP16 transgenic insertions for tissue-
730 specific cell labeling and ablation in zebrafish. Dev Biol *304*, 811–824.

731 Durán, I., Marí-Beffa, M., Santamaría, J.A., Becerra, J., and Santos-Ruiz, L. (2011). Actinotrichia
732 collagens and their role in fin formation. Developmental Biology *354*, 160–172.

733 Feitosa, N.M., Zhang, J., Carney, T.J., Metzger, M., Korzh, V., Bloch, W., and Hammerschmidt, M.
734 (2012). Hemicentin 2 and Fibulin 1 are required for epidermal-dermal junction formation and fin
735 mesenchymal cell migration during zebrafish development. Developmental Biology *369*, 235–248.

736 Fu, M., Vohra, B.P.S., Wind, D., and Heuckeroth, R.O. (2006). BMP signaling regulates murine
737 enteric nervous system precursor migration, neurite fasciculation, and patterning via altered Ncam1
738 polysialic acid addition. Developmental Biology *299*, 137–150.

739 Garriock, R.J., and Krieg, P.A. (2007). Wnt11-R signaling regulates a calcium sensitive EMT event
740 essential for dorsal fin development of Xenopus. Developmental Biology *304*, 127–140.

741 Goldstein, A.M., Brewer, K.C., Doyle, A.M., Nagy, N., and Roberts, D.J. (2005). BMP signaling is
742 necessary for neural crest cell migration and ganglion formation in the enteric nervous system.
743 Mechanisms of Development *122*, 821–833.

744 Hao, J., Ho, J.N., Lewis, J.A., Karim, K.A., Daniels, R.N., Gentry, P.R., Hopkins, C.R., Lindsley, C.W.,
745 and Hong, C.C. (2010). In vivo structure - Activity relationship study of dorsomorphin analogues
746 identifies selective VEGF and BMP inhibitors. ACS Chemical Biology *5*, 245–253.
747 Ka, J., Kim, J.D., Pak, B., Han, O., Choi, W., Kim, H., and Jin, S.W. (2020). Bone Morphogenetic
748 Protein Signaling Restricts Proximodistal Extension of the Ventral Fin Fold. Frontiers in Cell and
749 Developmental Biology *8*, 603306.
750 Kalluri, R. (2016). The biology and function of fibroblasts in cancer. Nature Reviews Cancer *16*, 582–
751 598.
752 Kendall, R.T., and Feghali-Bostwick, C.A. (2014). Fibroblasts in fibrosis: Novel roles and mediators.
753 Frontiers in Pharmacology *5 MAY*, 123.
754 Kuroda, J., Itabashi, T., Iwane, A.H., Aramaki, T., and Kondo, S. (2020). The Physical Role of
755 Mesenchymal Cells Driven by the Actin Cytoskeleton Is Essential for the Orientation of Collagen
756 Fibrils in Zebrafish Fins. Frontiers in Cell and Developmental Biology *8*, 580520.
757 Lalonde, R.L., and Akimenko, M.A. (2018). Effects of fin fold mesenchyme ablation on fin
758 development in zebrafish. PLoS ONE *13*, e0192500.
759 Lee, R.T.H., Knapik, E.W., Thiery, J.P., and Carney, T.J. (2013). An exclusively mesodermal origin of
760 fin mesenchyme demonstrates that zebrafish trunk neural crest does not generate ectomesenchyme.
761 Development (Cambridge) *140*, 2923–2932.
762 Ma, R.C., Jacobs, C.T., Sharma, P., Kocha, K.M., and Huang, P. (2018). Stereotypic generation of
763 axial tenocytes from bipartite sclerotome domains in zebrafish. PLoS Genetics *14*, e1007775.
764 Muhl, L., Genové, G., Leptidis, S., Liu, J., He, L., Mocci, G., Sun, Y., Gustafsson, S., Buyandelger, B.,
765 Chivukula, I. V, et al. (2020). Single-cell analysis uncovers fibroblast heterogeneity and criteria for
766 fibroblast and mural cell identification and discrimination. Nature Communications *11*, 3953.
767 Murayama, E., Sarris, M., Redd, M., Le Guyader, D., Vivier, C., Horsley, W., Trede, N., and
768 Herbomel, P. (2015). NACA deficiency reveals the crucial role of somite-derived stromal cells in
769 haematopoietic niche formation. Nature Communications *6*, 8375.
770 Nakamura, T., Gehrke, A.R., Lemberg, J., Szymaszek, J., and Shubin, N.H. (2016). Digits and fin rays
771 share common developmental histories. Nature *537*, 225–228.
772 Parichy, D.M., Elizondo, M.R., Mills, M.G., Gordon, T.N., and Engeszer, R.E. (2009). Normal table of
773 postembryonic zebrafish development: Staging by externally visible anatomy of the living fish.
774 Developmental Dynamics *238*, 2975–3015.
775 Pouget, C., Pottin, K., and Jaffredo, T. (2008). Sclerotomal origin of vascular smooth muscle cells and
776 pericytes in the embryo. Developmental Biology *315*, 437–447.
777 Rajan, A.M., Ma, R.C., Kocha, K.M., Zhang, D.J., and Huang, P. (2020). Dual function of perivascular

778 fibroblasts in vascular stabilization in zebrafish. PLoS Genetics *16*, e1008800.
779 Rocha, M., Beiriger, A., Kushkowski, E.E., Miyashita, T., Singh, N., Venkataraman, V., and Prince,
780 V.E. (2020). From head to tail: regionalization of the neural crest. Development (Cambridge, England)
781 *147*.
782 Saxena, M., Agnihotri, N., and Sen, J. (2018). Perturbation of canonical and non-canonical BMP
783 signaling affects migration, polarity and dendritogenesis of mouse cortical neurons. Development
784 (Cambridge) *145*, dev147157.
785 Schindelin, J., Arganda-Carreras, I., Frise, E., Kaynig, V., Longair, M., Pietzsch, T., Preibisch, S.,
786 Rueden, C., Saalfeld, S., Schmid, B., et al. (2012). Fiji: an open-source platform for biological-image
787 analysis. Nature Methods *9*, 676–682.
788 Schweitzer, R., Chyung, J.H., Murtaugh, L.C., Brent, A.E., Rosen, V., Olson, E.N., Lassar, A., and
789 Tabin, C.J. (2001). Analysis of the tendon cell fate using Scleraxis, a specific marker for tendons and
790 ligaments. Development (Cambridge, England) *128*, 3855–3866.
791 Sela-Donenfeld, D., and Kalcheim, C. (1999). Regulation of the onset of neural crest migration by
792 coordinated activity of BMP4 and Noggin in the dorsal neural tube. Development *126*, 4749–4762.
793 Sharma, P., Ruel, T.D., Kocha, K.M., Liao, S., and Huang, P. (2019). Single cell dynamics of
794 embryonic muscle progenitor cells in zebrafish. Development *146*, dev178400.
795 Smith, M.M., and Hall, B.K. (1990). Development and evolutionary origins of vertebrate skeletogenic
796 and odontogenic tissues. Biological Reviews of the Cambridge Philosophical Society *65*, 277–373.
797 Smith, M., Hickman, A., Amanze, D., Lumsden, A., and Thorogood, P. (1994). Trunk neural crest
798 origin of caudal fin mesenchyme in the zebrafish Brachydanio rerio. Proceedings of the Royal Society
799 B: Biological Sciences *256*, 137–145.
800 Sobkow, L., Epperlein, H.H., Herklotz, S., Straube, W.L., and Tanaka, E.M. (2006). A germline GFP
801 transgenic axolotl and its use to track cell fate: Dual origin of the fin mesenchyme during development
802 and the fate of blood cells during regeneration. Developmental Biology *290*, 386–397.
803 Subramanian, A., and Schilling, T.F. (2014). Thrombospondin-4 controls matrix assembly during
804 development and repair of myotendinous junctions. ELife *3*.
805 Tabib, T., Morse, C., Wang, T., Chen, W., and Lafyatis, R. (2018). SFRP2/DPP4 and FMO1/LSP1
806 Define Major Fibroblast Populations in Human Skin. The Journal of Investigative Dermatology *138*,
807 802–810.
808 Tallquist, M.D. (2020). Developmental pathways of cardiac fibroblasts. Cold Spring Harbor
809 Perspectives in Biology *12*.
810 Taniguchi, Y., Kurth, T., Medeiros, D.M., Tazaki, A., Ramm, R., and Epperlein, H.H. (2015).
811 Mesodermal origin of median fin mesenchyme and tail muscle in amphibian larvae. Scientific Reports

812 *5*, 11428.
813 Thulabandu, V., Chen, D., and Atit, R.P. (2018). Dermal fibroblast in cutaneous development and
814 healing. Wiley Interdisciplinary Reviews: Developmental Biology *7*.
815 Tucker, A.S., and Slack, J.M.W. (2004). Independent induction and formation of the dorsal and ventral
816 fins in Xenopus laevis. Developmental Dynamics *230*, 461–467.
817 Wattrus, S.J., and Zon, L.I. (2018). Stem cell safe harbor: The hematopoietic stem cell niche in
818 zebrafish. Blood Advances *2*, 3063–3069.
819 Wiegreffe, C., Christ, B., Huang, R., and Scaal, M. (2007). Sclerotomal origin of smooth muscle cells
820 in the wall of the avian dorsal aorta. Developmental Dynamics *236*, 2578–2585.
821 Wiley, D.M., Kim, J.D., Hao, J., Hong, C.C., Bautch, V.L., and Jin, S.W. (2011). Distinct signalling
822 pathways regulate sprouting angiogenesis from the dorsal aorta and the axial vein. Nature Cell
823 Biology *13*, 686–693.
824 Xie, T., Wang, Y., Deng, N., Huang, G., Taghavifar, F., Geng, Y., Liu, N., Kulur, V., Yao, C., Chen, P.,
825 et al. (2018). Single-Cell Deconvolution of Fibroblast Heterogeneity in Mouse Pulmonary Fibrosis. Cell
826 Reports *22*, 3625–3640.
827 Zhang, J., Wagh, P., Guay, D., Sanchez-Pulido, L., Padhi, B.K., Korzh, V., Andrade-Navarro, M.A.,
828 and Akimenko, M.A. (2010). Loss of fish actinotrichia proteins and the fin-to-limb transition. Nature
829 *466*, 234–237.
830

Figure 1

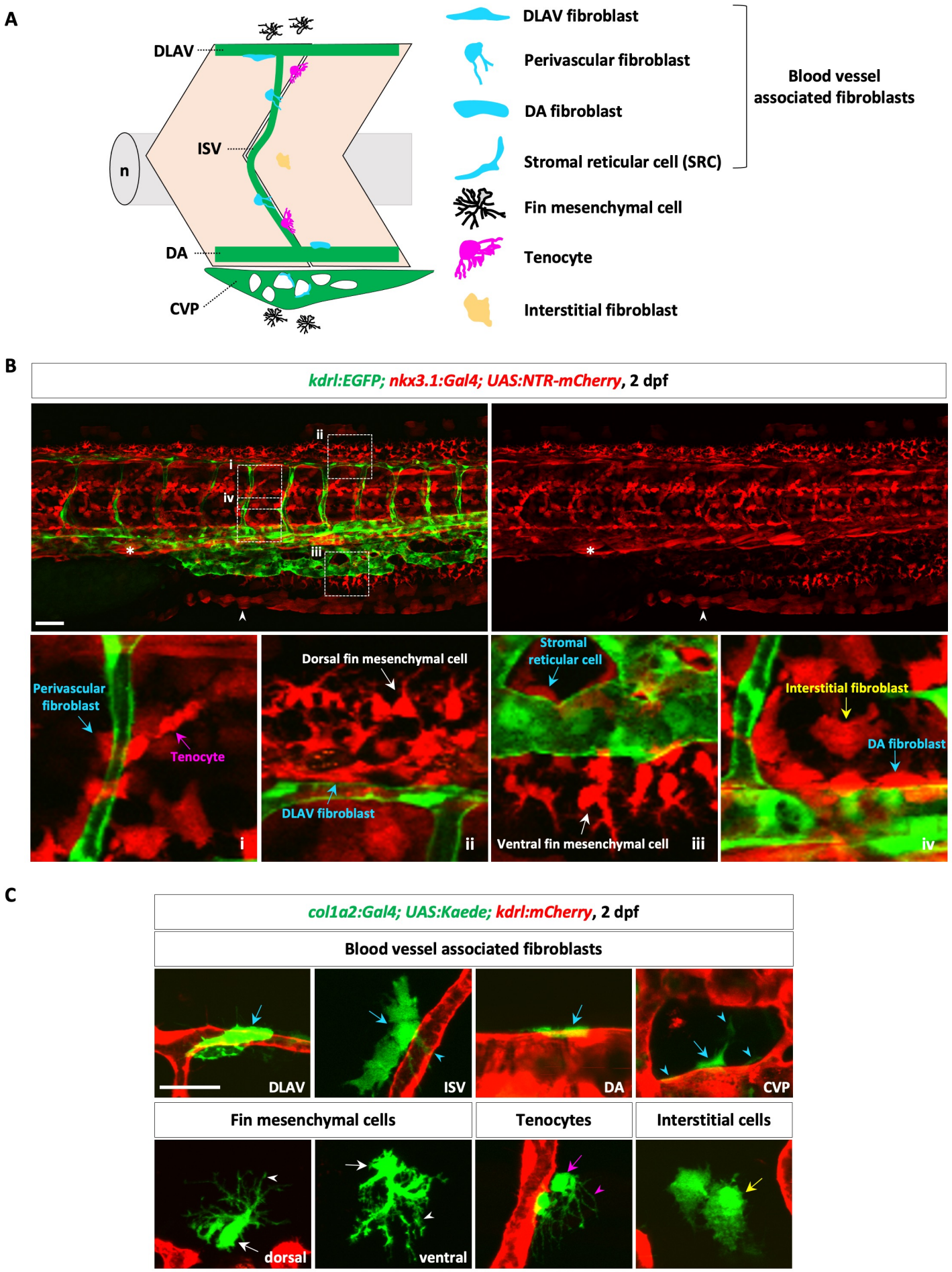
A
DLAV
ISV
n
DA
CVP
DLAV fibroblast
Perivascular fibroblast
DA fibroblast
Stromal reticular cell (SRC)
Blood vessel associated fibroblasts
Fin mesenchymal cell
Tenocyte
Interstitial fibroblast
B
kdrl:EGFP; nkx3.1:Gal4; UAS:NTR-mCherry, 2 dpf
i
ii
iii
iv
Perivascular fibroblast
Tenocyte
Dorsal fin mesenchymal cell
DLAV fibroblast
Stromal reticular cell
Ventral fin mesenchymal cell
Interstitial fibroblast
DA fibroblast
C
col1a2:Gal4; UAS:Kaede; kdrl:mCherry, 2 dpf
Blood vessel associated fibroblasts
DLAV
ISV
DA
CVP
Fin mesenchymal cells
Tenocytes
Interstitial cells
dorsal
ventral

Figure 2

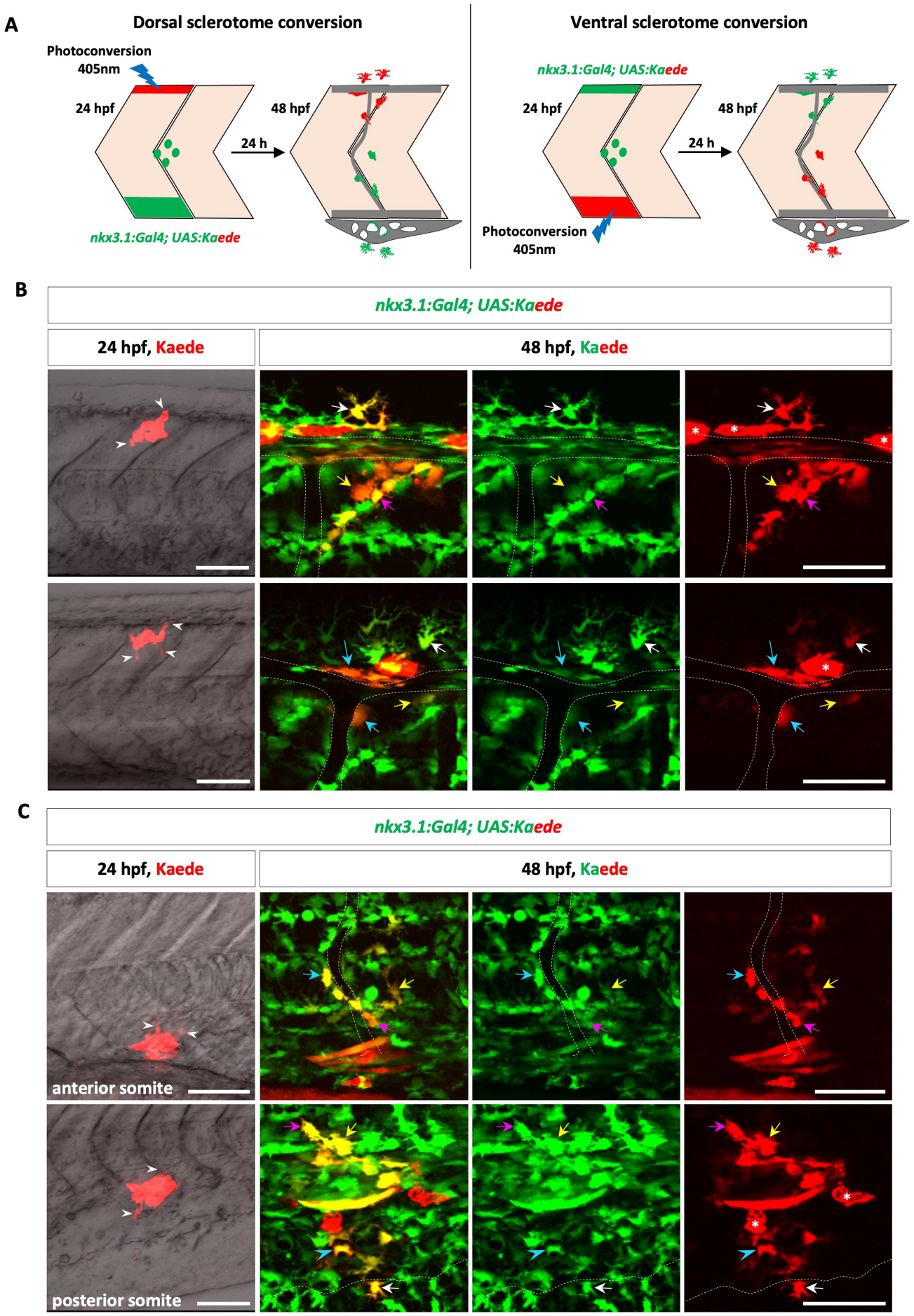
A
Dorsal sclerotome conversion
Photoconversion
405nm
24 hpf
48 hpf
24 h
nkx3.1:Gal4; UAS:Kaede
Ventral sclerotome conversion
nkx3.1:Gal4; UAS:Kaede
24 hpf
48 hpf
24 h
Photoconversion
405nm
B
nkx3.1:Gal4; UAS:Kaede
24 hpf, Kaede
48 hpf, Kaede
C
nkx3.1:Gal4; UAS:Kaede
24 hpf, Kaede
48 hpf, Kaede
anterior somite
posterior somite

Figure 3

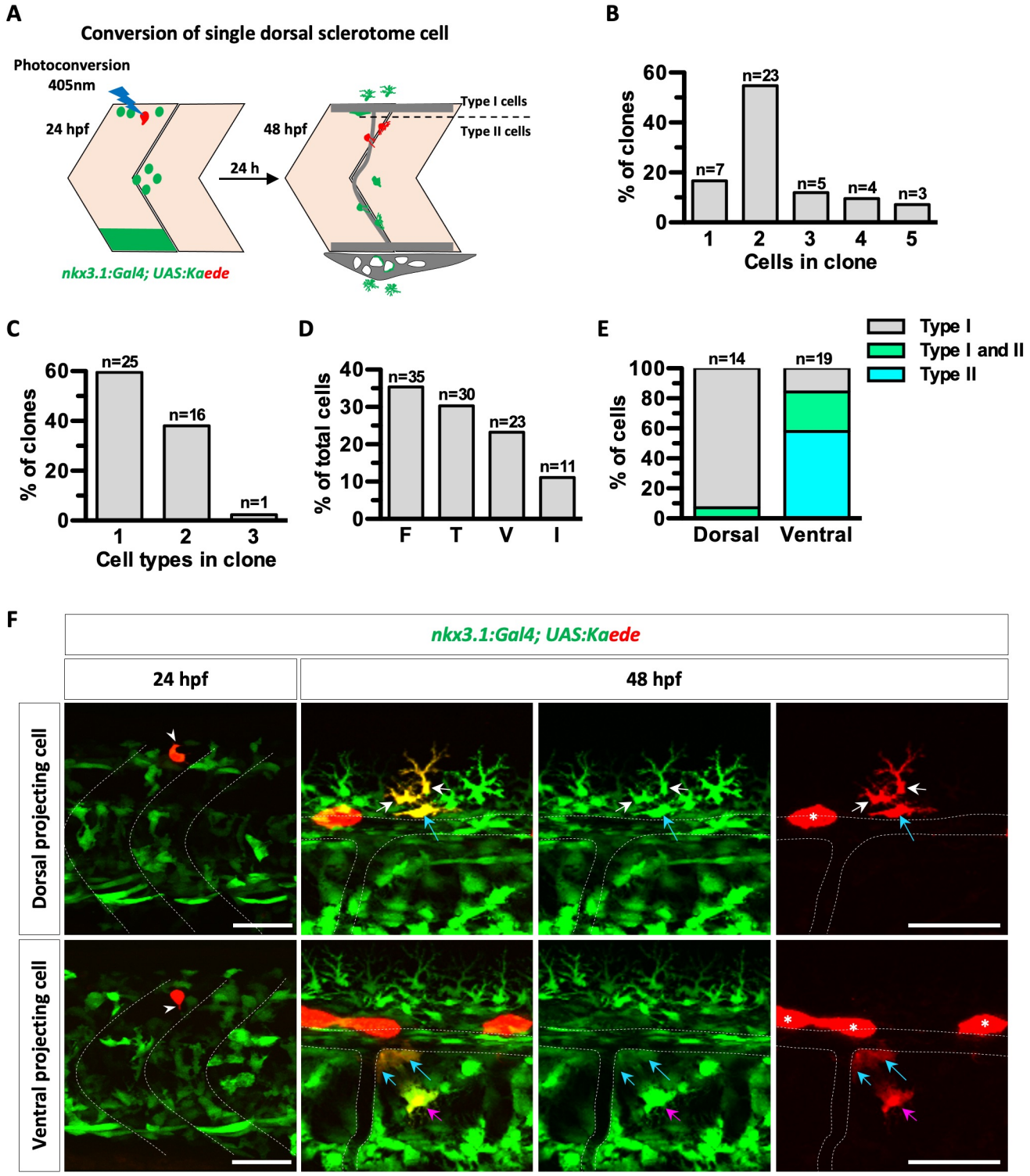
A
Conversion of single dorsal sclerotome cell
Photoconversion
405nm
24 hpf
24 h
48 hpf
Type I cells
Type II cells
nkx3.1:Gal4; UAS:Kaede
B
% of clones
Cells in clone
n=7
n=23
n=5
n=4
n=3
C
% of clones
Cell types in clone
n=25
n=16
n=1
D
% of total cells
F
T
V
I
n=35
n=30
n=23
n=11
E
% of cells
Dorsal
Ventral
n=14
n=19
Type I
Type I and II
Type II
F
nkx3.1:Gal4; UAS:Kaede
24 hpf
48 hpf
Dorsal projecting cell
Ventral projecting cell

Figure 4

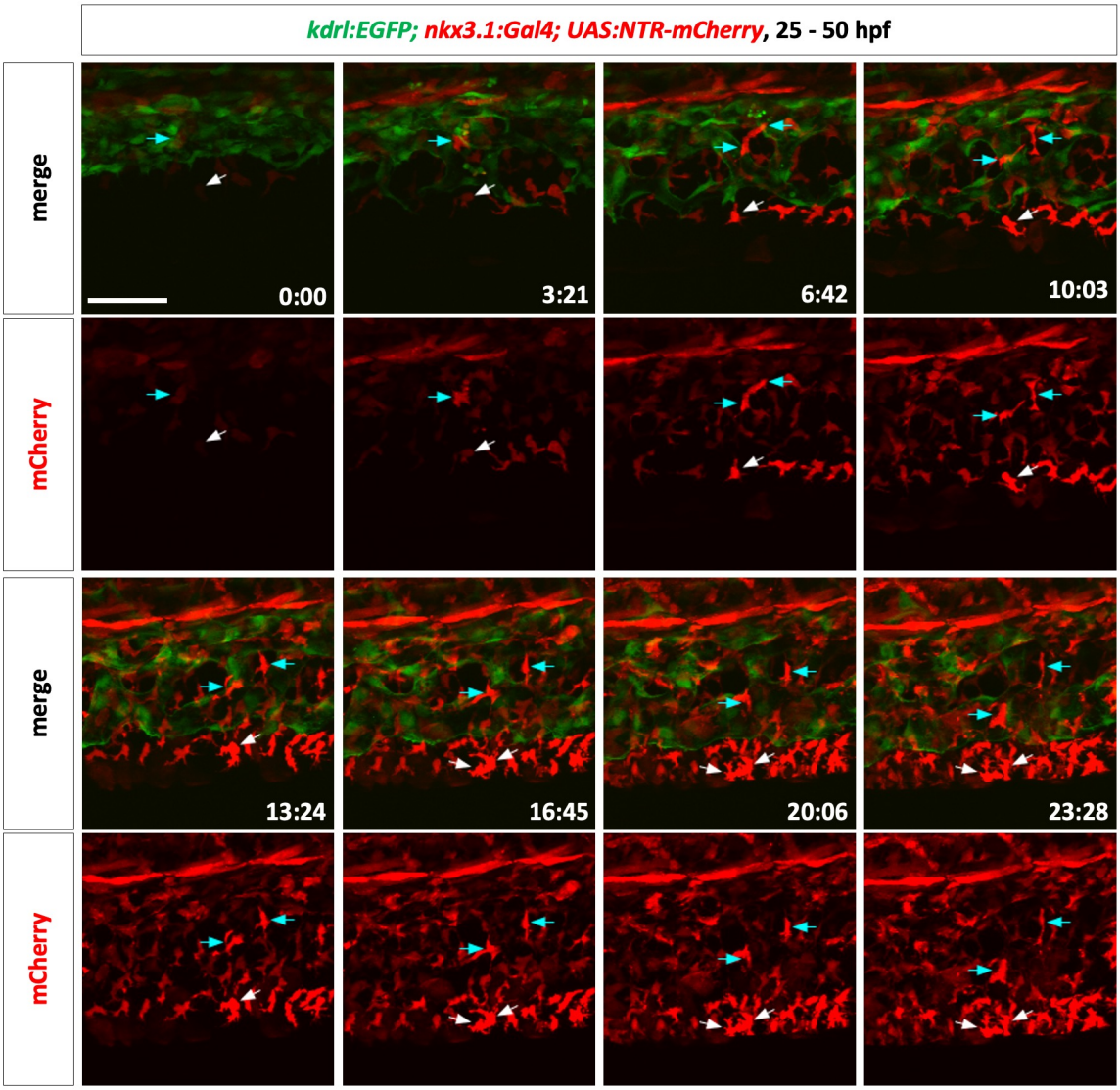
kdrl:EGFP; nkx3.1:Gal4; UAS:NTR-mCherry, 25 - 50 hpf
merge
mCherry
merge
mCherry
0:00
3:21
6:42
10:03
13:24
16:45
20:06
23:28

Figure 5

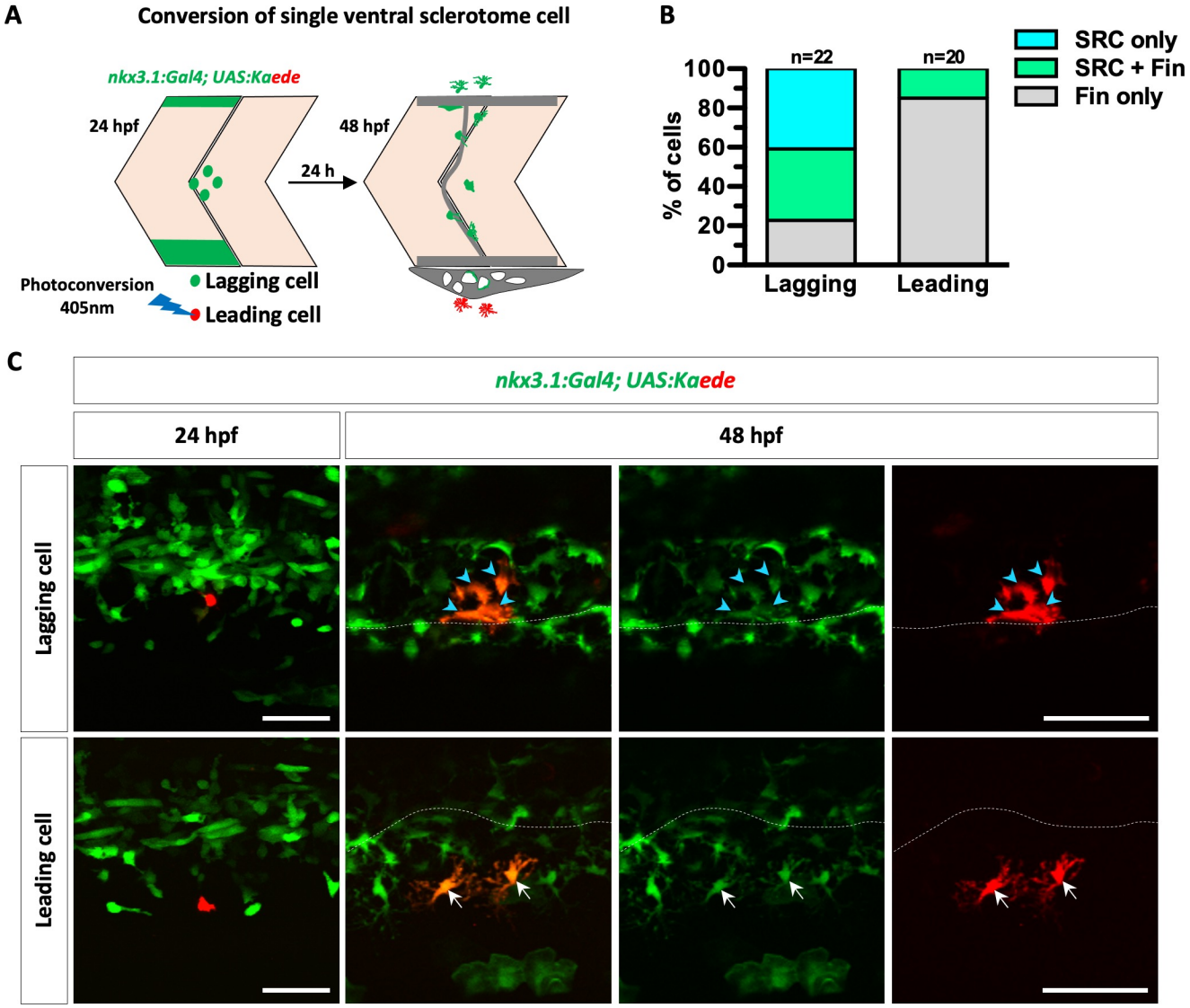
A
Conversion of single ventral sclerotome cell
nkx3.1:Gal4; UAS:Kaede
24 hpf
48 hpf
24 h
Photoconversion
405nm
Lagging cell
Leading cell
B
SRC only
SRC + Fin
Fin only
% of cells
100
80
60
40
20
0
n=22
n=20
Lagging
Leading
C
nkx3.1:Gal4; UAS:Kaede
24 hpf
48 hpf
Lagging cell
Leading cell

Figure 6

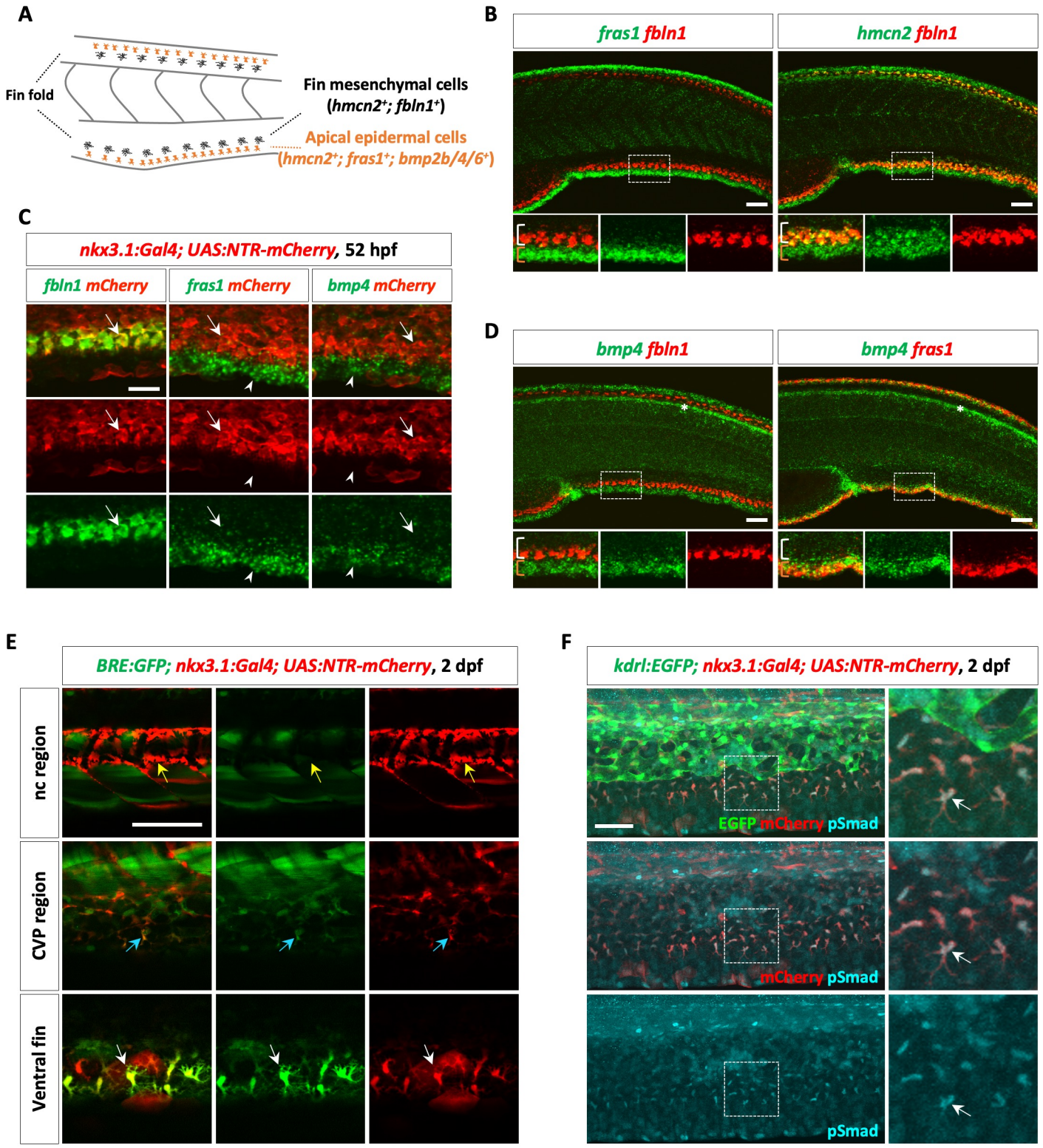
A
Fin fold
Fin mesenchymal cells
(hmcn2+; fbln1+)
Apical epidermal cells
(hmcn2+; fras1+; bmp2b/4/6+)
B
fras1 fbln1
hmcn2 fbln1
C
nkx3.1:Gal4; UAS:NTR-mCherry, 52 hpf
fbln1 mCherry
fras1 mCherry
bmp4 mCherry
D
bmp4 fbln1
bmp4 fras1
E
BRE:GFP; nkx3.1:Gal4; UAS:NTR-mCherry, 2 dpf
nc region
CVP region
Ventral fin
F
kdrl:EGFP; nkx3.1:Gal4; UAS:NTR-mCherry, 2 dpf
EGFP mCherry pSmad
mCherry pSmad
pSmad

Figure 7

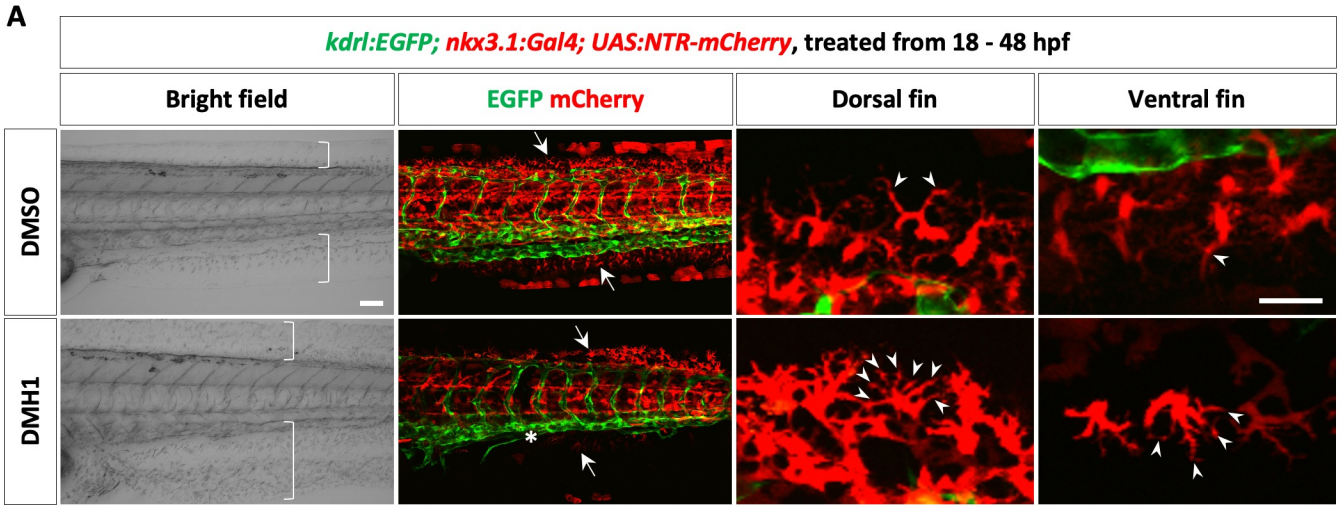
A
kdrl:EGFP; nkx3.1:Gal4; UAS:NTR-mCherry, treated from 18 - 48 hpf
Bright field
EGFP mCherry
Dorsal fin
Ventral fin
DMSO
DMH1

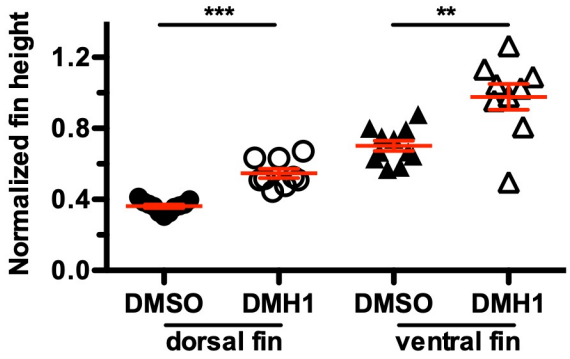
B
Normalized fin height
1.2
0.8
0.4
0.0
***
**
DMSO
DMH1
DMSO
DMH1
dorsal fin
ventral fin

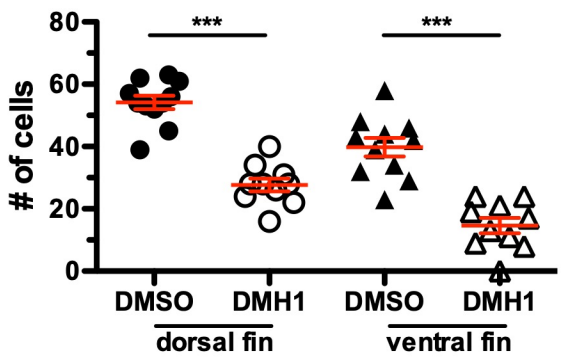
C
# of cells
80
60
40
20
0
***
***
DMSO
DMH1
DMSO
DMH1
dorsal fin
ventral fin

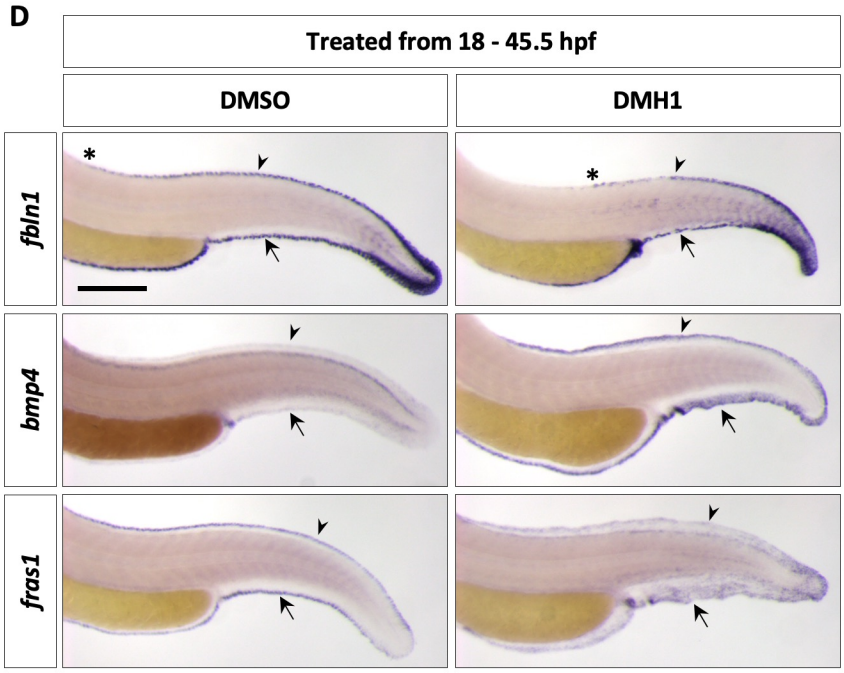
D
Treated from 18 - 45.5 hpf
DMSO
DMH1
fbln1
bmp4
fras1

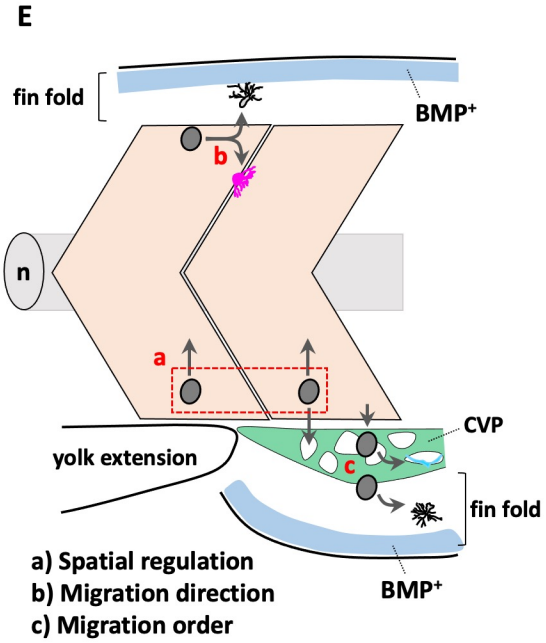
E
fin fold
BMP+
b
n
a
CVP
yolk extension
c
fin fold
BMP+
a) Spatial regulation
b) Migration direction
c) Migration order

Figure S1

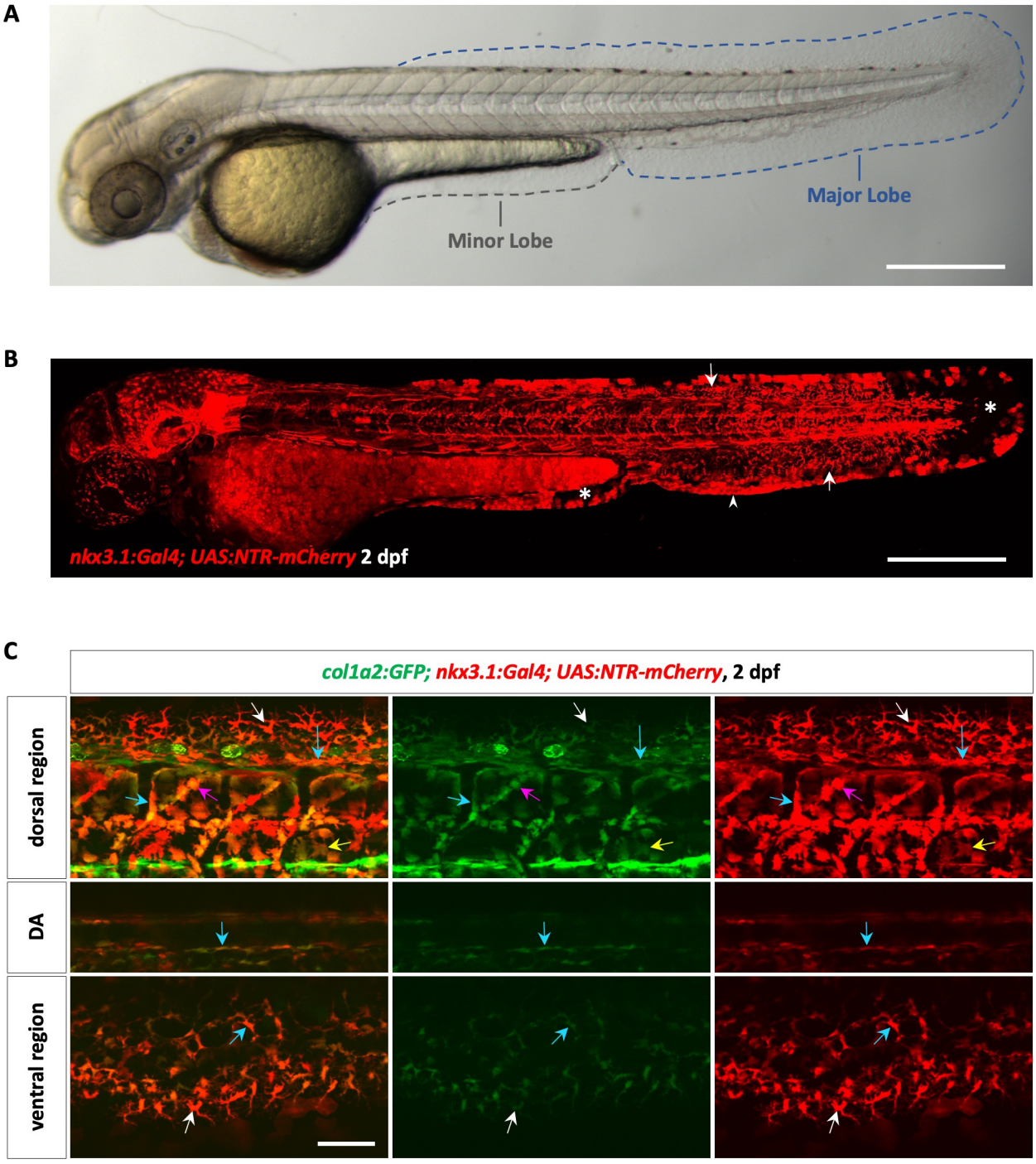
A
Major Lobe
Minor Lobe
B
nkx3.1:Gal4; UAS:NTR-mCherry 2 dpf
C
col1a2:GFP; nkx3.1:Gal4; UAS:NTR-mCherry, 2 dpf
dorsal region
DA
ventral region

Figure S2

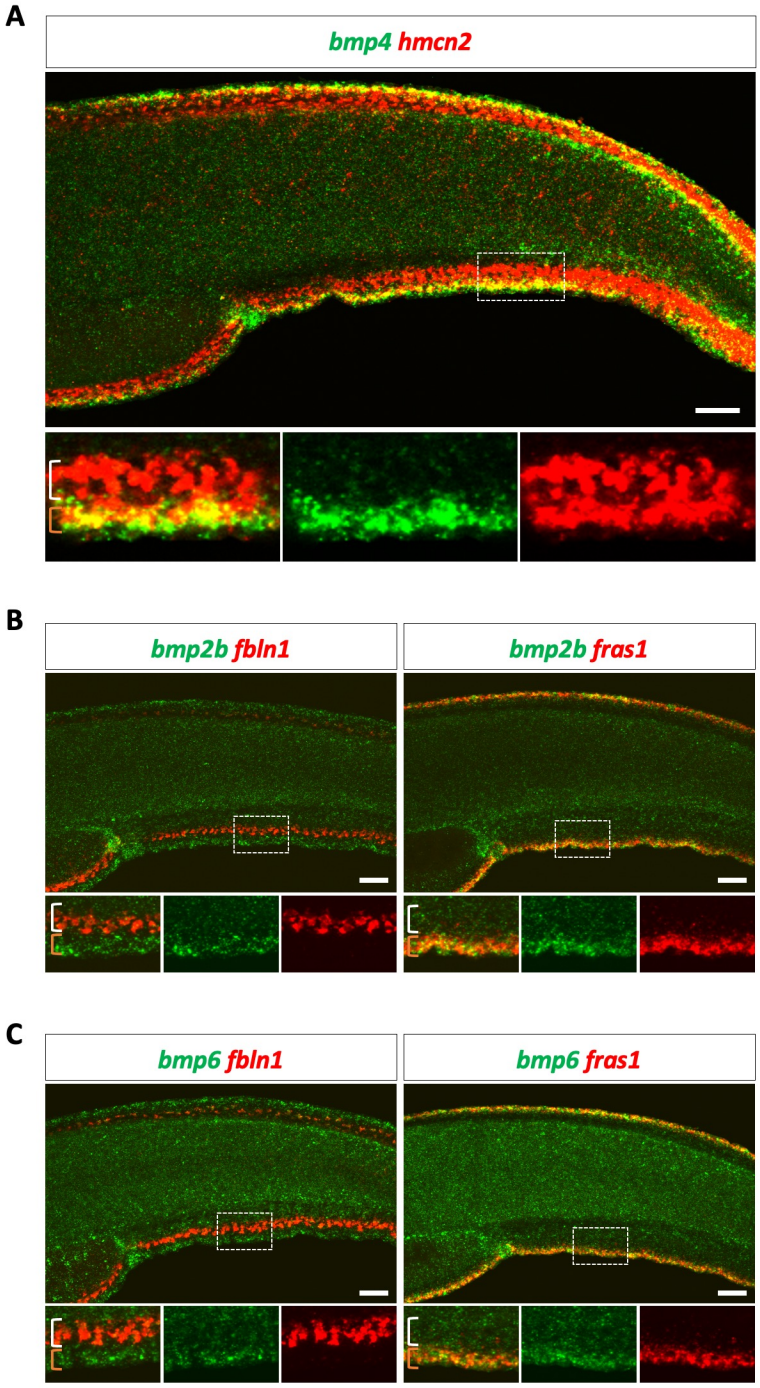
A
bmp4 hmcn2
B
bmp2b fbln1
bmp2b fras1
C
bmp6 fbln1
bmp6 fras1

Figure S3

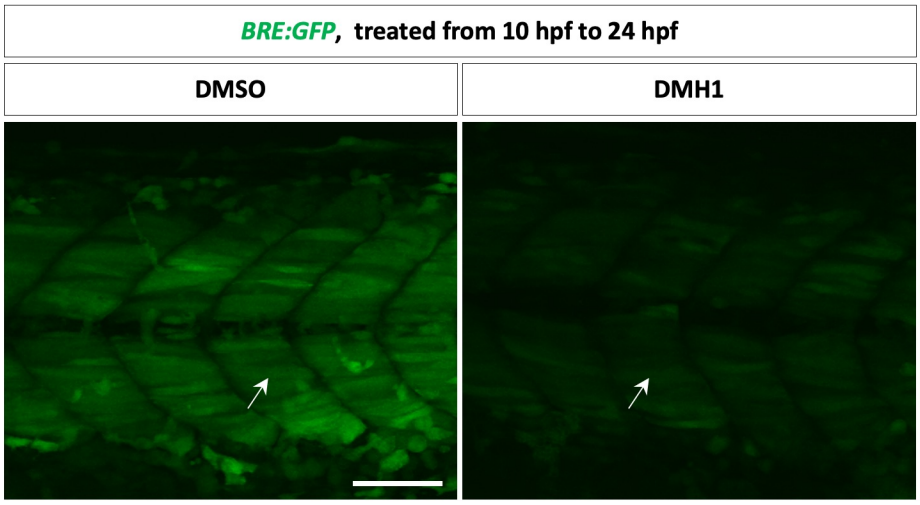

Figure S4

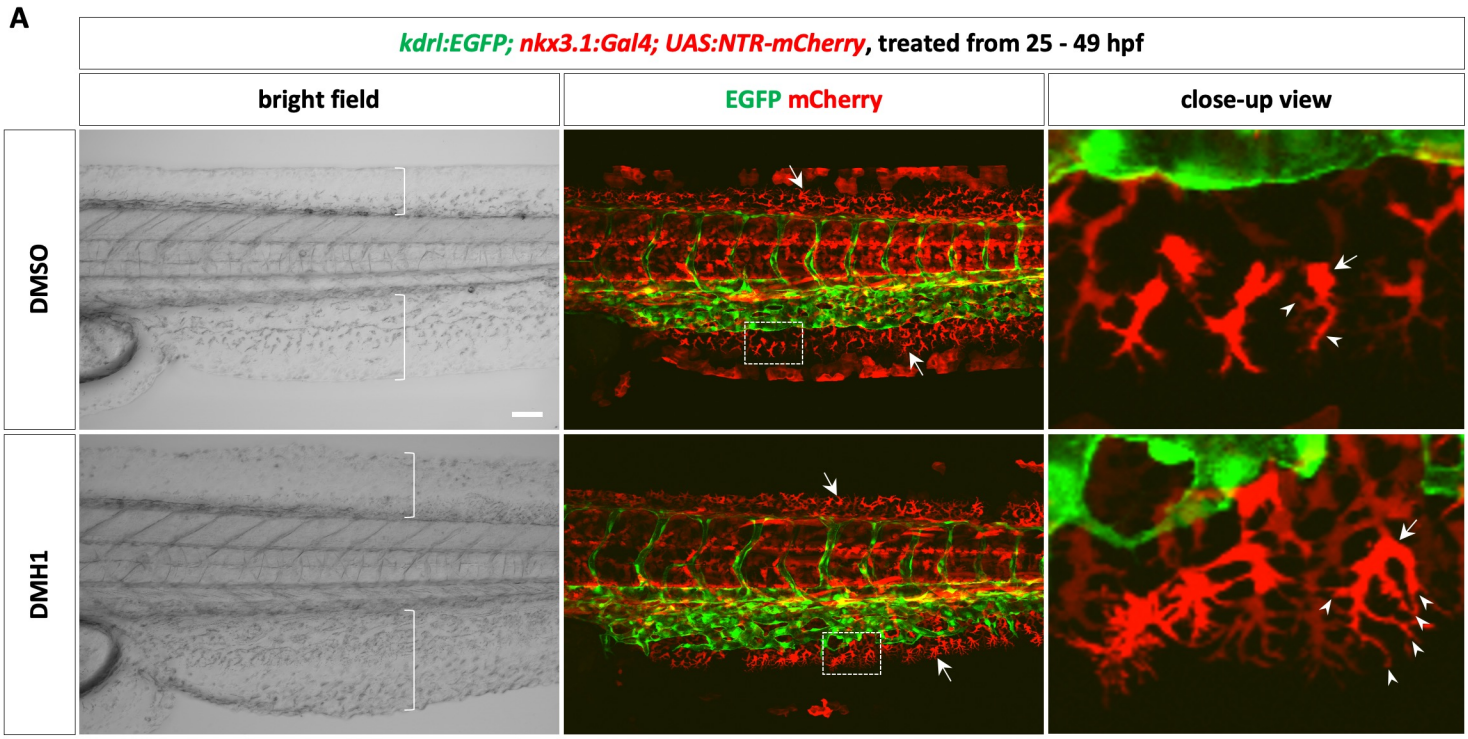
A
kdrl:EGFP; nkx3.1:Gal4; UAS:NTR-mCherry, treated from 25 - 49 hpf
bright field
EGFP mCherry
close-up view
DMSO
DMH1

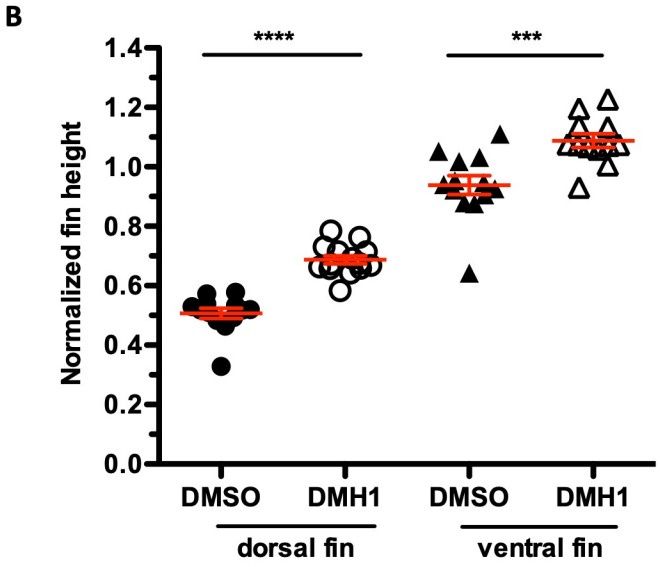
B
****
***
Normalized fin height
1.4
1.2
1.0
0.8
0.6
0.4
0.2
0.0
DMSO
DMH1
DMSO
DMH1
dorsal fin
ventral fin

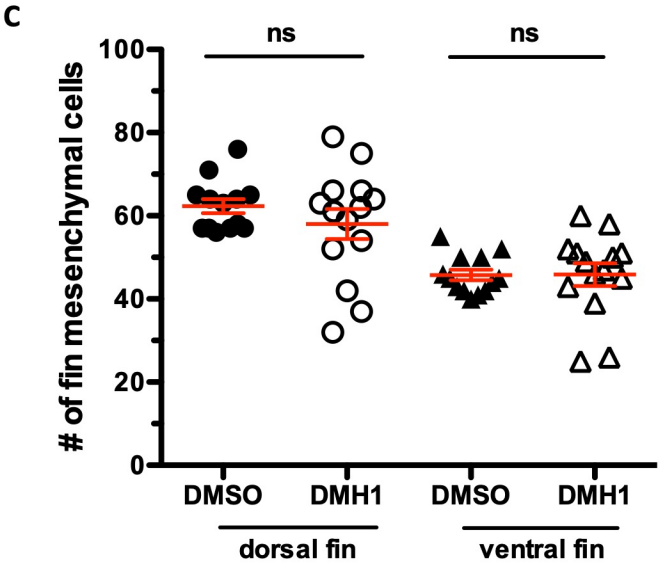
C
ns
ns
# of fin mesenchymal cells
100
80
60
40
20
0
DMSO
DMH1
DMSO
DMH1
dorsal fin
ventral fin